FEASIBILITY STUDY OF T700 ROTORCRAFT ENGINE ROTOR SUPPORTED BY HYBRID AIR FOIL BEARINGS

By

MAHESH KUMAR VARREY

Presented to the Faculty of the Graduate School of

The University of Texas at Arlington in Partial Fulfillment

Of the Requirements

For the Degree of

MASTER OF SCIENCE IN MECHANICAL ENGINEERING

THE UNIVERSITY OF TEXAS AT ARLINGTON

December 2011

DEDICATED TO ALMIGHTY AND MY FAMILY

ACKNOWLEDGMENTS

I would like to thank the committee head, my advisor Dr. Daejong Kim for his guidance throughout the course of this research. I would also like to thank Dr. Allan Bowling and Dr. Kent Lawrence for taking the time to serve on my committee.

I would also like to thank my colleagues at the Microturbomachinery and Energy Systems Laboratory along with my Roommates and friends at UTA for their help and support. I extend a special thanks to Texas Advanced Computing Center (TACC), for their support.

November 18, 2011

ABSTRACT

FEASIBILITY STUDY OF T700 ROTORCRAFT ENGINE ROTOR SUPPORTED BY HYBRID AIR FOIL BEARINGS

MAHESH KUMAR VARREY, M.S.

The University of Texas at Arlington, 2011

Supervising Professor: Dr. Daejong Kim

A potential solution towards light weighted and simple structured turbomachinery lies in elimination of oil-lubrication system. These promising benefits of oil-free turbomachinery have demanded extensive research in the field of small turbomachinery, leading to the development of different types of oil free bearings. Air foil bearings (AFBs) are one of the oil-free bearings with many advantages over others.

AFBs have simple construction, greater service life and reduced maintenance. Their superior dynamic performance compared to traditional rigid surface bearings is an added advantage. Implementation of these foil bearings in the rotorcraft propulsion system decreases the total weight of the engine setup, improving its performance. In addition it aids to reduce emissions.

This article is a feasibility study on compatibility of hybrid air foil bearings (HAFBs) with the T700 engine rotor under two different bearing designs. The HAFB was developed in Dr. Kim's laboratory over years, and HAFBs use external pressurized air supply during start/stop while they operate under either hydrodynamic condition or continuous hybrid mode at normal operating condition. The first design is with two 2 pad HAFBs and the second design is with two 3 pad HAFBs.

A multi-degree of freedom (DOF) nonlinear rotordynamic analysis of a rigid rotor model supported by two HAFBs has been presented. The non-linear equations of motion of the rotor have been solved to determine translational and gyroscopic motions, and time dependent Reynolds Equation was used to obtain the dynamic reaction forces and moments from the HAFBs.

A Visual C++ code has been developed to simulate the characteristic behavior of the rotor based on former discussed numerical model. The imbalance response for both in cylindrical and conical modes has been discussed. In addition, minimum film thickness of the bearings in both cylindrical and conical modes has been evaluated.

TABLE OF CONTENTS

LIST OF ILLUSTRATIONS

LIST OF TABLES

NOMENCLATURE

C_j: Nominal clearance of journal bearing

C: Radial clearance of the circular top foils journal bearing

C_{SB}: Set bore clearance

e: Eccentricity

e_x, e_y: Translational displacement of rotor

F_{X_B}, F_{Y_B}: Forces induced by journal bearings

M_{Ξ_B}, M_{ψ_B}: Moments induced by journal bearings

F_{X_U}, F_{Y_U}: Forces induced by imbalance of rotor

h_j: Film thickness of journal bearing

H_j: Nondimensional journal bearing film thickness, $H_j = \frac{h_j}{C_j}$

I_T: Translational moment of inertia

r_p: Bearing preload

R_P: Non Dimensionalized Bearing preload, $R_P = \frac{r_p}{C_j}$

I_P: Polar moment of inertia

m_r: Rotor mass

M_{Ξ_U}, M_{ψ_U}: Moments induced by imbalance mass

p_a: Ambient pressure

p_j: Pressure developed in journal bearing

P_j: Nondimensional pressure of journal bearing, $P_j = \frac{p_j}{p_a}$

r: Radial coordinate

r_{gc}: Centrifugal growth of rotor

R_{rot}: Radius of the rotor

t: Time

Z : Non-dimensional axial coordinate, $Z = \frac{z}{R}$

R_g : Gas constant of air

Greeks

*δ: T*op foil deflection

θ: Circumferential coordinate

Λ : Bearing number

μ: Viscosity of air

v: Poisson's ratio

$\rho_{r:}$ Density of rotor

φ_p: Angular location of added imbalance from reference

τ : Nondimensional time, $\tau = \omega t$

ξ, ψ : Angular displacement of rotor

ω : Rotating speed

ω_S : Excitation frequency

θ: Circumferential coordinate

CHAPTER 1

INTRODUCTION

Though oil lubrication is the most widely used method among the other means of lubrication, it has its own disadvantages such as periodical maintenance, greasy machinery, work space consumption and other intricate problems. A potential solution to these problems lies in the oil-free turbomachinery. A rotorcraft propulsion system implemented with oil-free turbomachinery has better performance due to its lighter weight, compact design and extreme temperature capability. Cleaner operating environment is an additional benefit of employing an oil-free turbomachinery.

Hence keen interest in the research towards the elimination of the oil-lubrication system lead to the development of oil free bearing viz. the air foil bearing, magnetic bearing and hybrid foil magnetic bearing. However, these bearings demand a lot more research to know the technological limit.

1.1. Types of oil-free bearings

Typically oil-free bearings can be classified into air foil bearings, magnetic bearings and a combination of both i.e. the hybrid foil magnetic bearings.

1.1.1. Magnetic Bearings

The magnetic bearing shown in Figure 1.1 uses the principle of electromagnetism. The rotor is lifted off through the attractive electromagnetic forces produced by the coils placed around it in the stator. The orbit of the rotor is maintained with the help of the position sensors, which provide a feedback to the controller placing the rotor in the desired orbit and position. One main advantage of them is the high dynamic stiffness and damping.

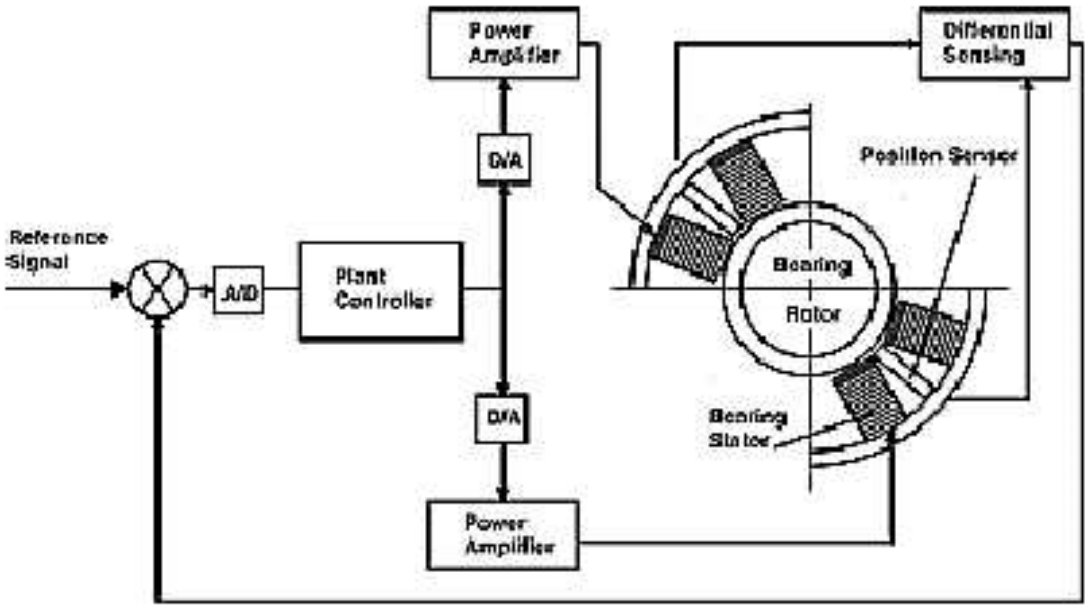

Figure 1.1. Schematic of a Magnetic bearing showing its feedback control [SKF magnetic bearings]

1.1.2. Air Foil Bearings

The air foil bearings (AFBs) shown in Figure 1.2 have a compliant structure with a top foil arranged in a bearing sleeve. These compliant structures are of different types; the most common one is the corrugated bump foil as shown in the figure supporting the smooth top foil. The working fluid is air in most cases. Their capacity to work in extreme temperatures and their robust design found them a place in high-speed aerospace rotating machinery such as air cycle machines (ACMs), auxiliary power units (APUs) [1].

These bearings work by building hydrodynamic pressure in the air film. This can be explained with two effects, the wedge effect and the squeeze film effect. The wedge effect explains the pressure builds between the two converging surfaces, i.e., the stationary bearing and the rotating journal. The squeeze film effect builds the pressure due to the resistance shown by the gas molecules in the film when squeezed suddenly. These foil bearings work impressively at higher speeds and have high load carrying capability [2], than rigid walled air

bearings. The design characteristics of AFB's also accommodate for minor rotor misalignments increasing their reliability.

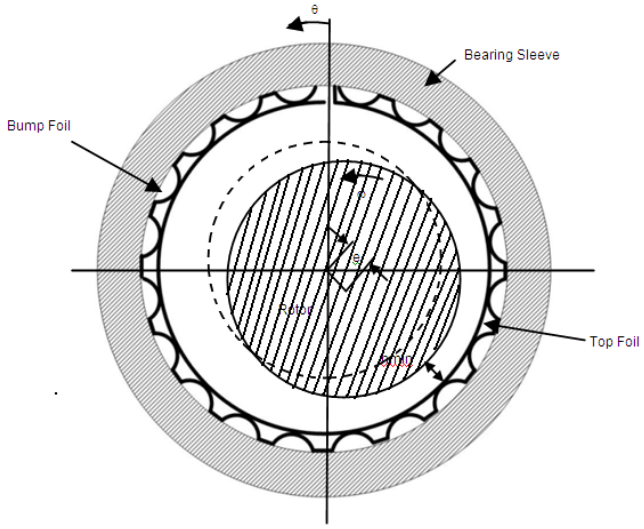

Figure 1.2. Schematic of a rotor with certain eccentricity with respect to air foil bearing with continuous circular top foil and corrugated bump foils.

Though AFBs are remarkable at high speeds and have high load carrying capacities, they have problems relating to thermal runaway due to lack of heat dissipation capability and frictional wear during start/stop. To overcome these issues, hybrid air foil bearings (HAFBs) have been introduced, which operate on both hydrodynamic and hydrostatic pressurization. The theory behind the HAFBs has been greatly supported with the experimental work conducted at Dr.Kim's Laboratory over years. More details on HAFBs are presented in Section 2.4.

1.1.3. Hybrid Foil and Magnetic Bearing

This bearing is a combination of both the AFB and the magnetic bearings. As shown in Figure 1.3, the magnetic bearings lift the rotor at zero or low speeds and the foil bearings bolster it at high speeds. They have high load capacity, high static stiffness and control versatility.

Swanson et al [3] have tested two types of Foil-magnetic hybrid bearing, a nested configuration where foil bearing components have been inserted in the radial gap available in the active magnetic bearing (AMBs) and a side-by-side arrangement. Test results for system operation during simulated failure of AMB were positive, proving the capability of the AFB in supporting the shaft in an emergency.

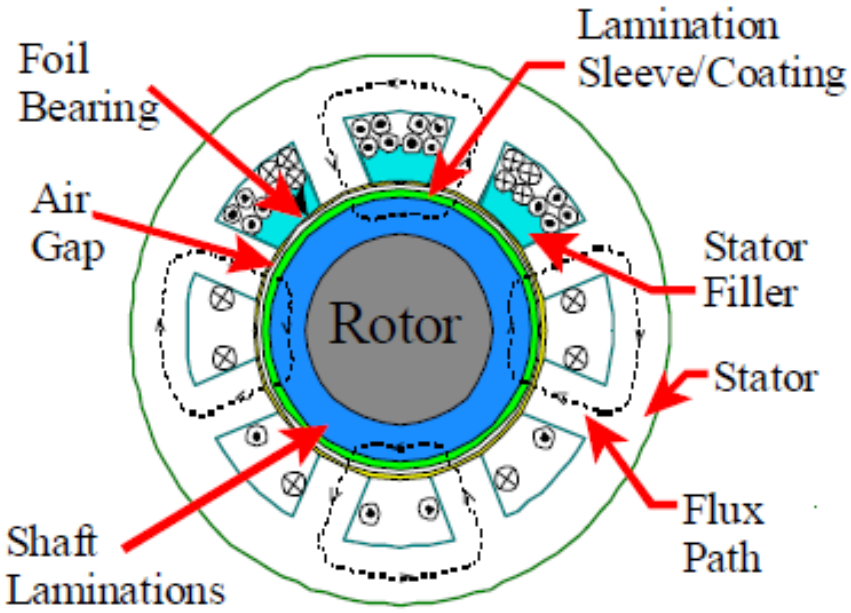

Figure 1.3. Schematic of a Nested Hybrid Foil/Magnetic Bearing

CHAPTER 2

ARCHITECTURE OF T700 ENGINE

2.1. General Description of T700 Rotorcraft Engine

The T700 is a turboshaft engine developed by the General Electric for the U.S. Army Utility Tactical Transport Aircraft System (UTTAS). The Engine of the T700 is constructed and maintained according to four different modules, controls and compressor, cold-section, hot-section and power turbine.

The engine is 47” in length, 23” in height, and 25” in width. The engine is constructed from corrosion resistant steel except for a titanium axial compressor casing, aluminum inlet separator frame and a magnesium gearbox case. The Cut-section view of the T700 engine is shown in Figure 2.1

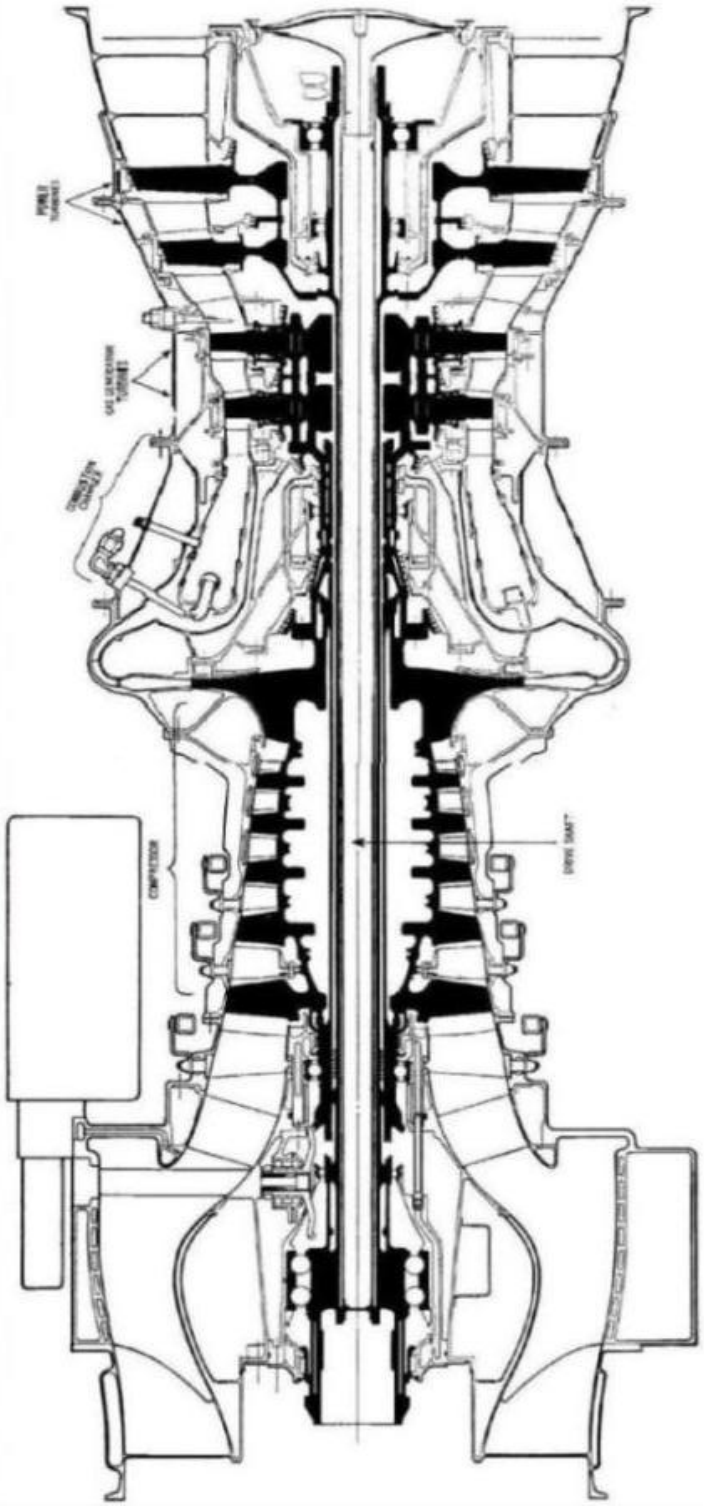

Figure 2.1 Cut-section View of T700 Rotorcraft Engine.

2.1.1. Compressor

The compressor comprises of five-axial and one centrifugal stage. The centrifugal impeller is mounted on the same shaft as the axial compressor. The compressor has a total of 332 blades, less in number compared to the blade count on currently manufacture engines. The solid model of the rotor in the subsection 2.2 was designed with the same blade count. The rotor stage blades and discs of the axial compressor are single piece castings leading to a better stability.

Gas Generator turbine

The manual [4] says “It is a two-stage, air cooled, high-performance, axial-flow turbine with a modular design making it easy to maintain. The sub modules contain first stage turbine nozzle with 24 air-cooled cast vane segments paired together, held in place with retaining rings and bolts and turbine rotor."

2.1.2. Power Turbine

It is a two stage tip-shrouded design with replaceable turbine blades and nozzle segments. The output shaft governing speed range is from 17,000 rpm to 23,000 rpm with a maximum rated speed of 24,000 RPM. Third and fourth stage discs are mounted on the drive shaft, which is a hollow unit splined to the shorter output shaft at the forward end supported by bearings [4].

2.1.3. Bearing Arrangement

The drive shaft is supported by four journal bearings. The engine rotor is supported by two rolling element bearings, one (angular contact ball bearing taking axial load) in the cold section and the other (roller bearing) in the hot section. Circumferential carbon seals and labyrinth seals are used on the power turbine shaft and gas generator turbines respectively. The replacement of these rolling element bearings supporting the engine rotor with foil bearings and their feasibility is discussed in the current paper.

2.1.4. Lubrication System

An oil lubrication system, built into the inlet particle separator, provides with the necessary lubrication for the bearings. In order to keep the bearing form failing the continuous supply of oil is ensured with the help of an emergency lubrication system built into the design, with small reservoirs bearing sumps. Air jets also provide with the mist lubrication wherever there is an oil leak [4].

2.2. Research Activities at NASA Glen Research Center on T700

NASA has been carrying out extensive research in foil bearing in collaboration with the U.S. Army. In their research towards advancing on the state-of-the-art in Oil-free turbo machinery, NASA, Glen research center has been exploring the various applications of AFB's in turbochargers, aircraft air cycle machines and turbocompressors.

NASA proposed a four-step process for the integration of the Foil bearings into the turbomachinery [5]. The steps are as follows: 1) Conducting Feasibility study of the application, by performing rotordynamic analysis through computer generated values. 2) Testing the candidate bearings built according to the simulated values obtained from the code. 3) Simulating the rotordynamic system with the designed bearings analyzing their stability, 4) Developing a prototype and then Testing it. These steps serve as the general outline and each step has to be evaluated well.

NASA engineers applied the above stated four step process to develop oil-free version of T700 rotorcraft engines.

Howard et al [6] have carried out the first step, finding the feasibility of the Foil bearings integration into the T700 model with a system level analysis on its compatibility. They have built a baseline rotordynamic model of the T700 configured with a gas generating turbine driving a compressor on a high-speed rotor, and a lower speed power turbine driving an output shaft coupled to a transmission [6] . Their baseline rotordynamic model closely resembles the actual

engine, matching with its critical speeds and mass properties. This baseline model incorporated with the foil bearings was used for the analysis.

Two types of configurations of the Baseline model were scrutinized, 1) The baseline geometry stayed intact except for the changes made in accommodating the Foil bearings as shown in Figure 2.2; 2) The engine shaft made stiffer and the aft bearing relocated behind the turbine as shown in Figure 2.3 [6]. Feasibility of these two configurations was checked with the most influencing factors such as adequate load capacity and tolerable rotordynamic behavior. A simple Rule of Thumb model to estimate general AFB's load capacity developed by Dellacorte and Valco [7] was implemented to find approximate dimensions of the foil bearings to be used.

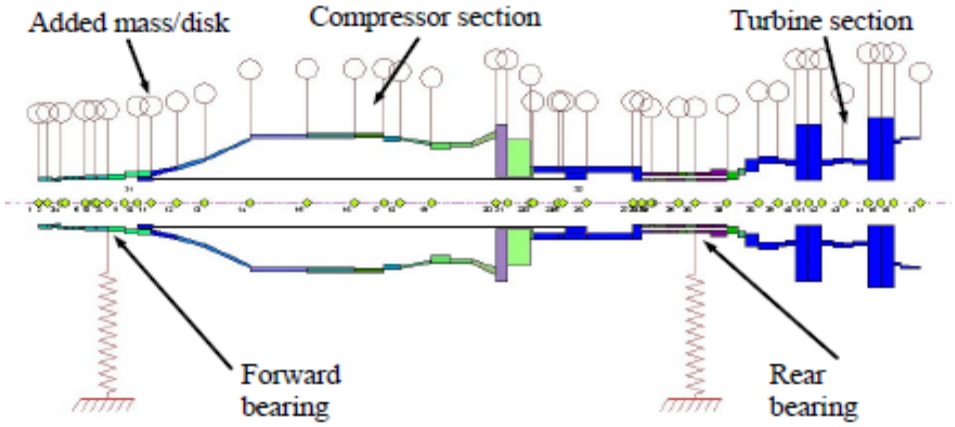

Figure 2.2 Rotordynamic model of baseline engine configuration I

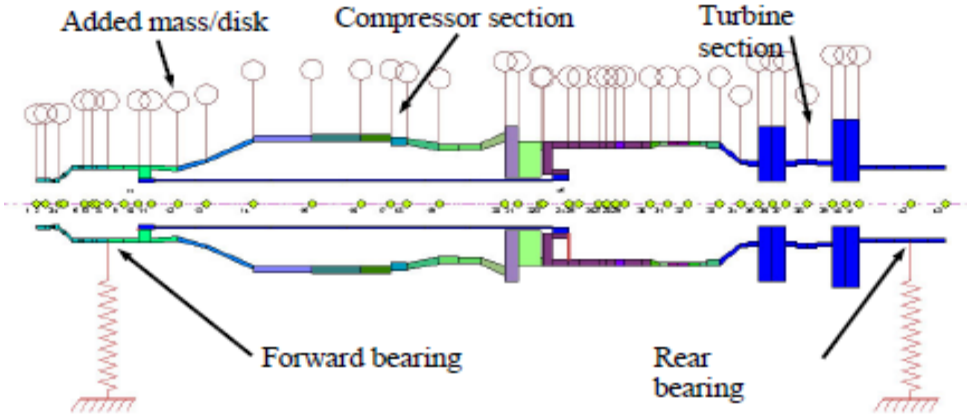

Figure 2.3 Rotordynamic model of baseline engine configuration II

General rotordynamic behavior of the two baseline engine configurations can be found once appropriate bearing stiffness and damping coefficients are inputted to the model. NASA engineers[6] used a computer code developed by Carpino and Talmage, to calculate the stiffness and damping coefficients of the AFBs, which are used as inputs for rotordynamic analysis software that gives the critical speed maps. The rotordynamic stability of the baseline configuration was analyzed and predicted with the critical speed maps. These numerical tests concluded that integration of foil bearings into the rotorcraft engines might be plausible.

Radil and Dellacorte [8] have performed durability tests on the rotorcraft-sized Airfoil bearing operating against a journal coated with PS304, a solid lubricant shaft coating developed by [9]. These bearings were tested for resilience on bases of damage to bearing's top foil, high temperature coating wear and delamination, recommending rapidly accelerated start-up's for a better bearing lift-off speed.

The step two in the four-step design process on testing the candidate bearings has been performed by Howard et al [10]. They have further researched and analyzed in the previous feasibility study [6], considering the foil bearing only on the hot section of the engine with a roller bearing element of the baseline model type 1 configuration from [6] .Two types of load tests have been performed; 1) Applying a steady load of 170 N (static load to be supported for T700 application) and checking if it could lift-off, 2) Applying a dead-weight load to check for the torque, power loss and periodical change in the temperatures. Through the data obtained a power loss map was constructed at a steady state temperature, to check for the corresponding power loss at the measured Torque at an RPM of 18000. Then a final coast-down test was conducted which also yielded reasonable results thereby qualifying the design dimensions of 76.2-by 63.4mm air foil bearing to be applicable in a T700 engine.

Radill et al [11] have examined the role of the radial clearance on the performance of Air-Foil bearings. Their studies show that an optimum radial clearance is very much necessary for the bearing to have a good load capacity. It was observed that the bearing would be

subjected to heavy thermal runaway if it has a smaller clearance than required and the load carrying capacity would go down by 20% if the clearance were more than the optimum.

2.3. Issues of NASA's Approach

Stiffness and damping have always been listed as the major properties, which have to be considered while analyzing a bearing support in the rotordynamic system. Many commercial softwares such as XL-Rotor, RODYN have been implementing this traditional method of rotordynamic analysis. NASA carried the feasibility analysis for foil bearings considering the same approach. This has been true to every rolling-element journal bearing, but when foil bearings have to be scrutinized for the feasibility of a particular rotor dynamic system, there is another major trait that has to be considered; non linear behavior of foil bearings and the film thickness of the bearing. The film thickness cannot be computed by any commercial software available if they use bearing stiffness and damping coefficients. Only a time domain transient analysis of the rotordynamic system can predict the film thickness values, which is more accurate than the stability analysis using the stiffness and damping coefficients.

As discussed by Radil et al [11] , if the radial clearance of the bearing is not optimum there is a greater chance in the reduction of load carrying capacity of the bearing. In addition the bearing is subjected to severe wear. The damping is adversely affected in case of a heavy film thickness as it limits the shaft motion to the soft air film loosing the effect of coulomb damping at the support structure.

A study of the five-degree of freedom non-liner rotordynamic analysis of a rigid rotor supported by a pair of air foil bearings and a thrust bearing has been performed by Lee and Kim [12]. They have investigated the effects of the variation of axial stiffness of the journal bearings on the minimum film thickness during critical speeds in conical modes of vibration, and the effect of a thrust bearing and thrust load on the rotordynamic behavior.

The film thickness has to be observed carefully as it varies with different modes of vibration. As analyzed by Lee and Kim[12], the conical mode of vibration had a minimum film

thickness at the edge of the bearing compared to cylindrical mode, leading to wear at the edges of the bearing.

Typically industrial machines with foil bearings are characterized by rapid acceleration to the normal operating speed to avoid prolonged dry rubbing at start/stop. The issue of exacerbated wear of the foil bearing due to slow acceleration of the rotorcraft engine has not been addressed properly. The current feasibility study employs HAFBs to support the rotorcraft engine, which provides a hydrostatic lift to the rotor solving the dry rubbing issues during the slow acceleration. In addition, T700 engine has a start motor connected to the front side of the rotor through a bevel gear mechanism, and the external loading from the gear train is another disadvantage of the traditional foil bearing during start up.

2.4. Preliminary work on hybrid foil bearing at UT-Arlington

Interest towards the construction of large air foil bearings arose from its application in gas-processing and military purposes. Lee and Kim [13] designed a Three-pad hybrid air foil bearing of diameter 101.6 mm shown in Figure 2.4 for the AFRL (Air Force Research Laboratory) test rig. Extensive preliminary rotordynamic analysis and parametric studies were performed to optimize the bump stiffness and also investigate on static performance at zero running speed.

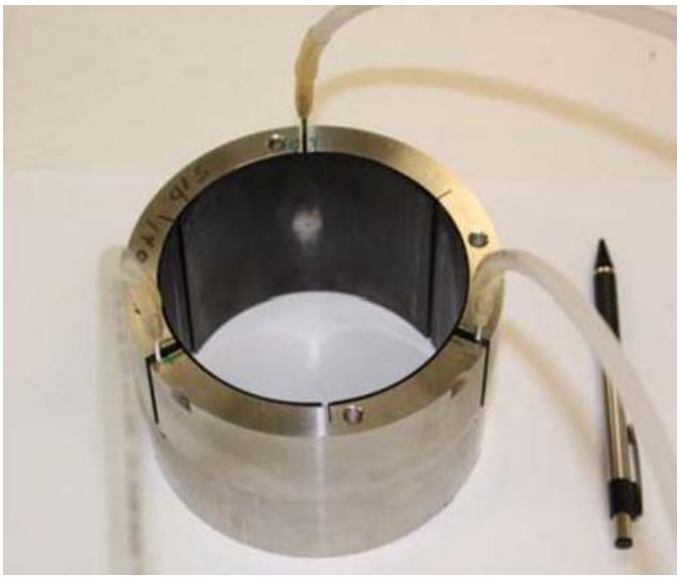

Figure 2.4 Photo of manufactured HAFB

As a continuation to the work done by Lee and Kim[13], the HAFB was further tested for its thermal behavior and start/stop friction at the Microturbomachinery and Energy Systems Laboratory. The test rig used by the researchers is shown in Figure 2.5. No damage of the top foil was recorded other than the break-in wear mark after 1000 start/stop cycles under 365 N at 5.52 bar supply pressure. All the tested speeds reached a thermal steady state within an hour.

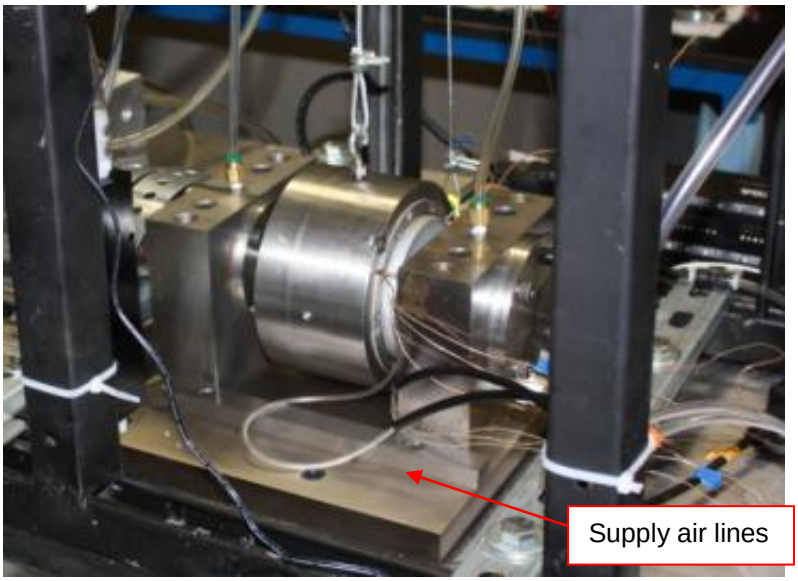

(a)

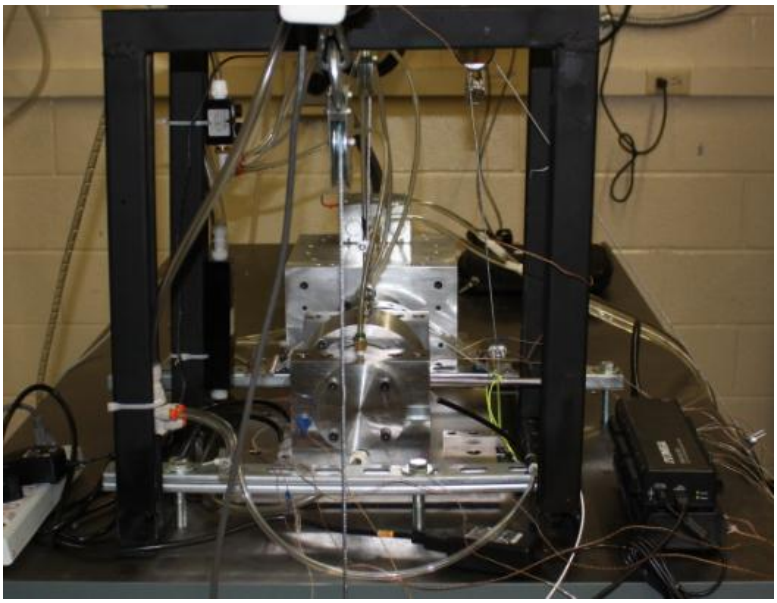

(b)

Figure 2.5 Photo of test rig for load capacity measurement at low speed (a) Side view (b) Front view

2.4.1. Principle of hybrid foil bearing

Externally pressurized hydrostatic air is fed into the annulus between the rotor and the bearing surface through the orifice tubes attached to the top foil as shown in the Figure 2.6.

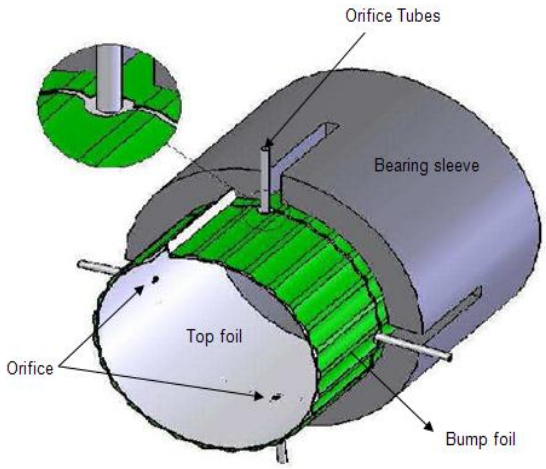

Figure 2.6 Schematic of a single pad HAFB[14]

This externally pressurized air provides a hydrostatic lift to the rotor, enabling it to overcome the issues concerning dry rubbing at stat/stop operations. Additionally the high pressurized air introduced into the bearing also acts as a coolant, dissipating the parasitic heat energy generated at high speed operation.

The bearings presented in this article have 3 pad and 2 pad configuration. Figure 2.7 shows the Schematic of a 3 pad HAFB showing set bore clearance and preload.

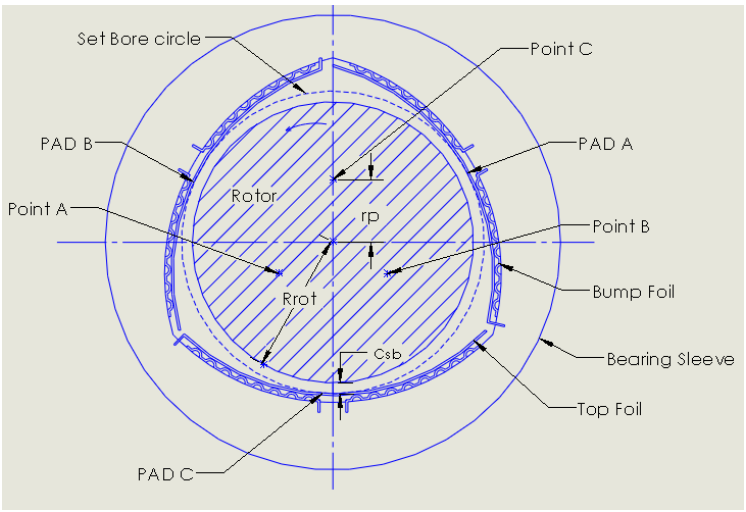

Figure 2.7 Schematic of a 3 pad HAFB configuration showing set bore clearance and preload.

Set bore clearance (C_{SB}) is the difference in length between the journal bearing clearance and the preload (r_p). It can be observed from Figure 2.7 that, the bearing and rotor are concentric with each other if preload is zero. The 3 pad bearing consists of 3 top foils and 6 bump foils. 3 orifices, one in the center of each pad are provided for pressurized air inlet, typically at an angle of 120°. The 2 pad bearing (not shown in the thesis due to proprietary design) consists of 2 top foils with total four orifices.

It was shown by Lee and Kim [12] that increases in external air supply pressure increases the critical speed of synchronous vibrations. Parametric study on HAFBs conducted by Kumar and Kim [15] shows that the cross coupled stiffness are also reduced, making the bearing more stable.

2.5. Project Objective

The present study is to investigate the feasibility of hybrid air foil bearings (HAFBs) with the T700 engine rotor under two different bearing designs. The first design is with two pad HAFBs and the second design is with three pad HAFBs.

A multi-degree of freedom (DOF) nonlinear rotordynamic analysis of a rigid rotor model supported by two HAFBs has been presented. The non-linear equations of motion of the rotor

have been solved to determine translational and gyroscopic motions, and time dependent Reynolds Equation was used to obtain the dynamic reaction forces and moments from the HAFBs.

A Visual C++ code has been developed to simulate the characteristic behavior of the rotor based on former discussed numerical model. The imbalance response for both in cylindrical and conical modes has been discussed. In addition, minimum film thickness of the bearing when the rotor passes both cylindrical and conical critical speeds has been evaluated.

CHAPTER 3

REVERSE ENGINEERING OF T700 AND MODIFICATION

In order to simulate the T700 engine configuration supported by HAFBs and perform a feasibility study, the rotor geometry is very essential. This chapter describes the method adopted to reverse engineer the T700 rotorcraft engine rotor from the available data. It also presents the effort put forth in redesigning the engine rotor to increase its bending critical speed so that it is above the operating speed range. In addition it has been designed with a provision for thrust bearing for future purpose.

3.1. Reverse engineering of T700 rotor

A complete rotordynamic study on the prospects of the Airfoil bearings supporting the core rotor in the candidate engine can be explored only if the complete dimensions and the built of the rotor are known. Due to the classified nature of the subject, it has been a challenge to find the dimensions of the rotor from the very little source of information available leading to the idea of reverse engineering the T700 rotor from the data at hand.

The reverse engineering has been possible from the cut-section view of the T700 engine in Figure 2.1and from the dimension of shaft diameter at front bearing, given as 50.8 mm in ref[6]. The cut-section view of the T700 engine is a scaled down model of the actual engine, which has been developed to the real life size by magnifying the image and adjusting the diameter of the rotor at the front bearing to match with the known diameter. This scale up view has been printed onto a paper and the rest of the unknown dimensions of the shaft have been measured with a ruler.

A 3D model of the T700 rotor has been developed with SolidWorks from the measured dimensions. The modeling of the rotor was done in different sections in order to facilitate the ease in editing the dimensions of the shaft as desired. The whole rotor was divided into

16sections axially; each section has been modeled to the dimensions obtained.. The blades of the five-stage axial compressor and the two-stage power turbine have also been modeled and placed in their respective sections. The blade count on each stage of the five-stage compressor has been followed as mentioned in ref [4]. This maintains the approximate mass properties when compared to the actual rotor. Finally the material properties of the parts created have been edited, choosing the properties of Duranickel ® 301 for the complete rotor shaft. The final model of the rotor is shown in Figure 3.1

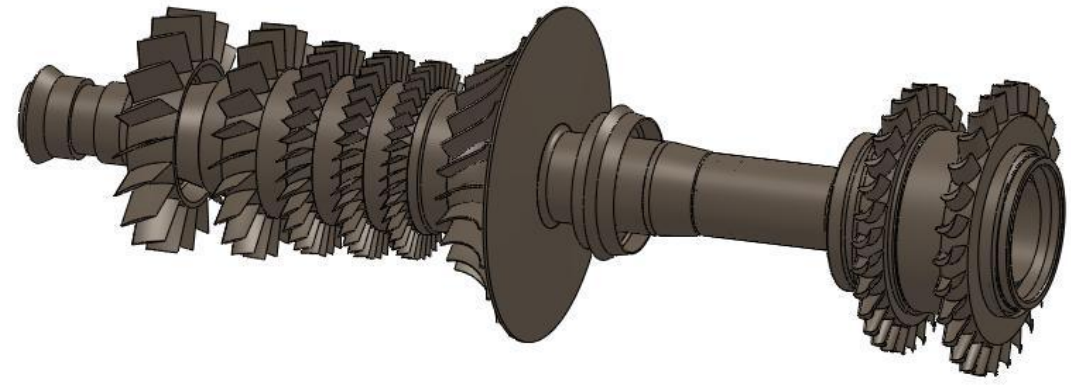

(a)

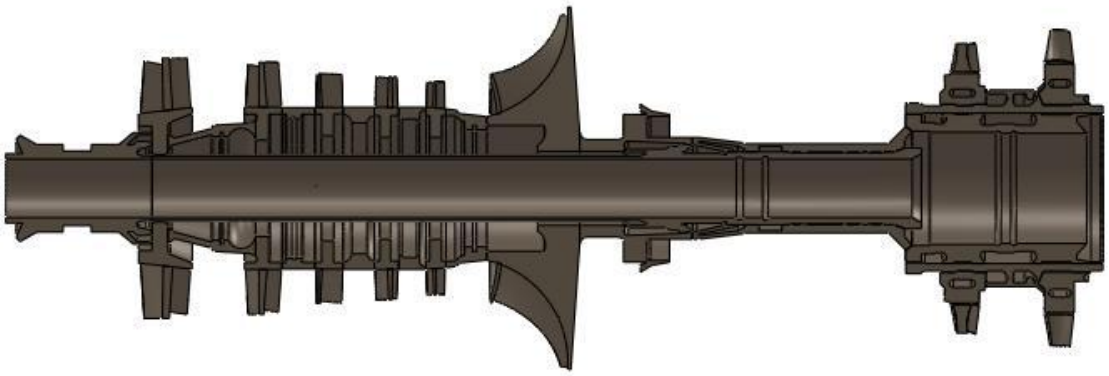

(b)

Figure 3.1 Solid model of T700 engine rotor (a) Diametric view (b) Front section view

The weight of the complete rotor assembly model has been found to be 23.45 kg through the mass properties tool, which was further reduced to 22.6 Kg reconsidering few dimensions. The final design of baseline model has an error of 1.8% compared to the actual weight of the T700 rotor discussed in ref [6].

A rotordynamic model of the baseline 3D model of T700 engine has been created in XLRotor ®. XLRotor is a rotordynamic analysis tool that takes the geometry of the shaft, material properties, mass properties, bearing dimensions as its input and generates the critical speed maps along with mode shapes as outputs.

The modeling of the rotor has been done considering it to be a flexible rotor, i.e. a number of lumped inertias connected by mass less elastic shafts. Hence the rotor is divided into 42 segments along its length as shown in Figure 3.2, and these segment geometries have been entered as the inputs for XLRotor ®. The material properties of the shaft such as, density, elastic's modulus and shear modulus have been given as 8200 Kg/m^3, 2*10^{11}N/m^2, and 7.7*10^{10} N/m^2 respectively. The input data for the added mass properties have been obtained from all the extra material of the shaft along the rotor, which does not contribute to the stiffness.

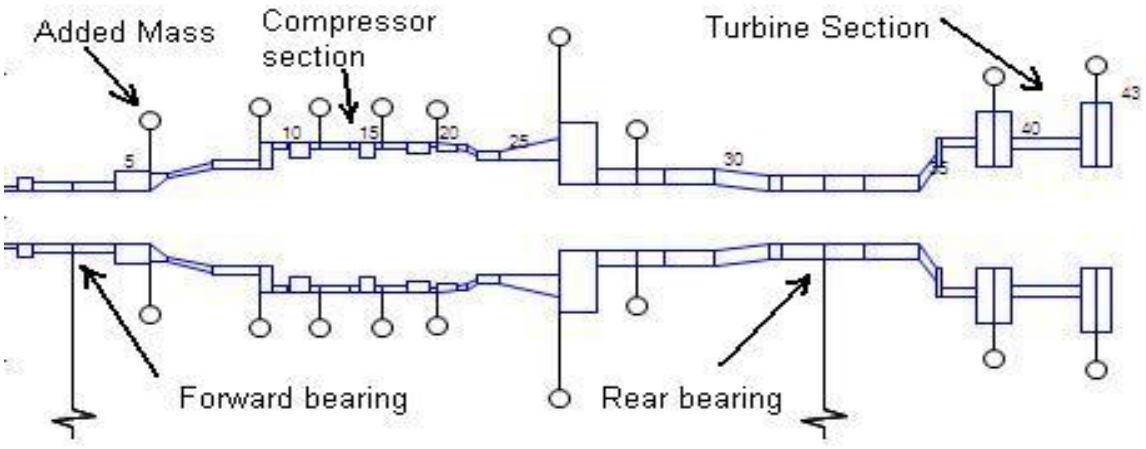

Figure 3.2 Rotordynamic model of baseline engine configuration

Standard rolling element bearing with a stiffness of 8,00,000 N/m have been chosen to support the rotor at both ends, and then the undamped critical speed map shown in Figure 3.3 has been obtained.

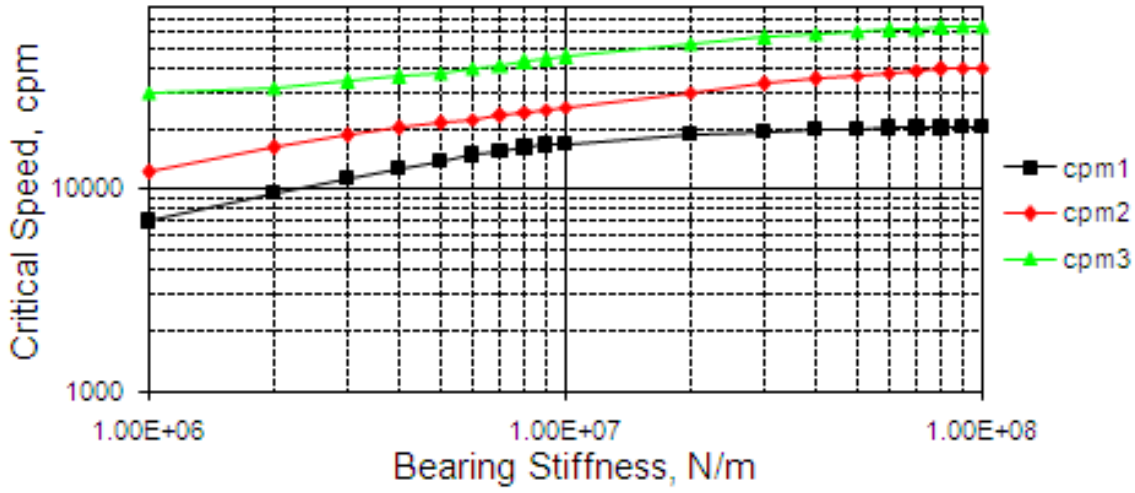

Figure 3.3. Undamped critical speed map for baseline configuration.

Similar rotordynamic behavior has been observed between the baseline rotordynamic model and the actual T700 engine [6], shown in Table 3.1

Table 3.1 Critical speed and mass comparison of baseline model to actual engine.

	The baseline model predicted values	Error compared to actual engine, percent
1st critical speed	6249 RPM	0.3
2nd critical speed	11017 RPM	-10.3
3rd critical speed	29654 RPM	12.8
Mass	22.4 Kg	1.8

Thus the preliminary goal of obtaining a baseline model of the T700 engine that is in good correlation with the actual engine has been achieved.

On careful evaluation of the obtained undamped critical speeds one can observe that, for the engine to reach its operating speed range the rotor has to pass through the 3rd critical speed (bending critical speed). Though the operating speed range is free of bending critical speeds, the vibrations at the compressor and turbines passing through the 3rd critical speed require large impeller tip clearances with shroud. The mode shape of the 3rd critical speed is overlapped on the rotordynamic model as seen in Figure 3.4.

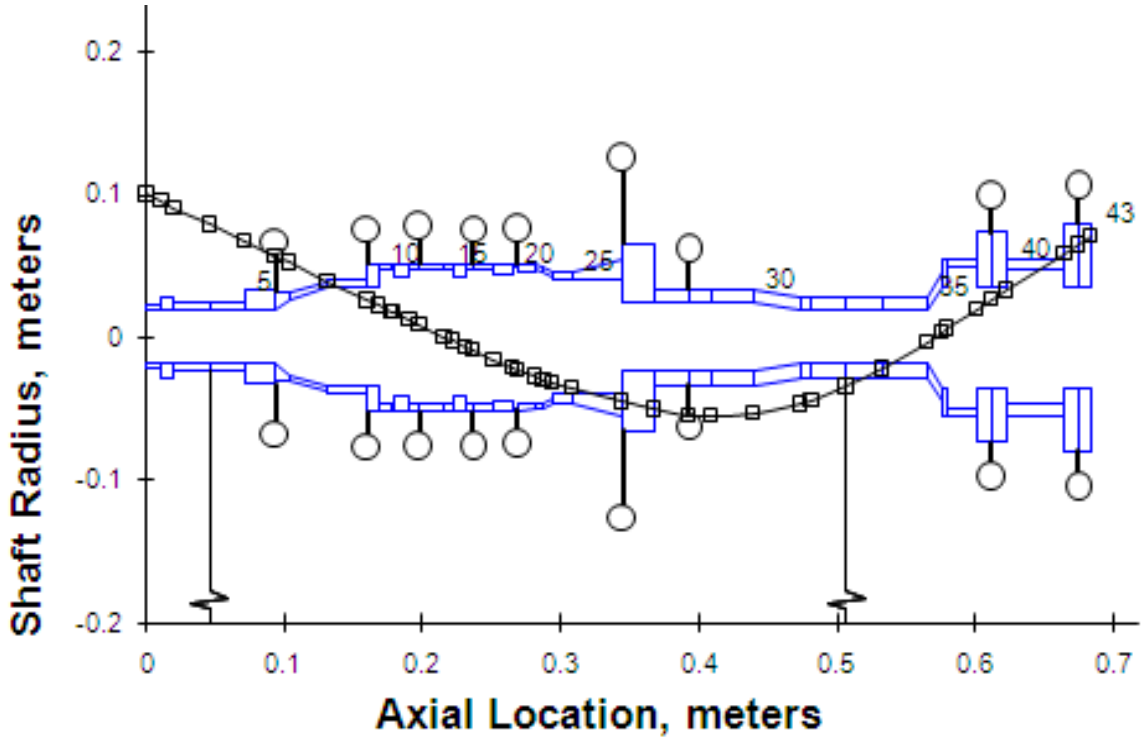

Figure 3.4 Mode shape plot of 3rd critical speed for baseline configuration

3.2. Modification of T700 rotor

Efforts have been made to redesign the rotor to increase the third critical speed (bending mode) so that it is above the operating speed range. To push the bending critical speed above the operating speed range, the engine shaft is made stiffer. A stiffer shaft has been achieved by increasing the overall shaft thickness, Inner diameter (ID) of the shaft from stage 5 to radial compressor, the outer diameter (OD) of the shaft near the hot-section by 45mm and decreasing the length of the shaft by 3cm at the hot-section as shown in Figure 3.5

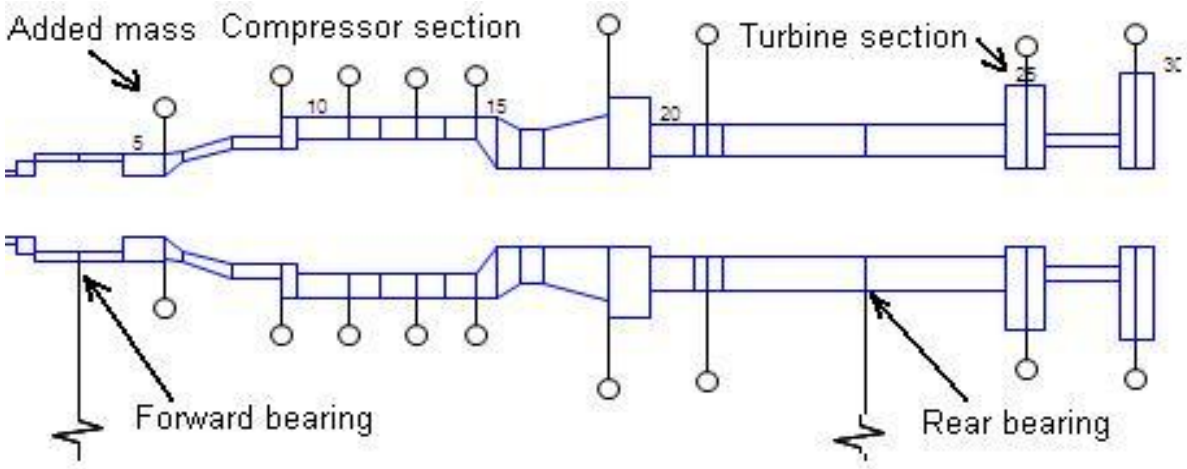

Figure 3.5 Rotordynamic model of stiffened engine design configuration

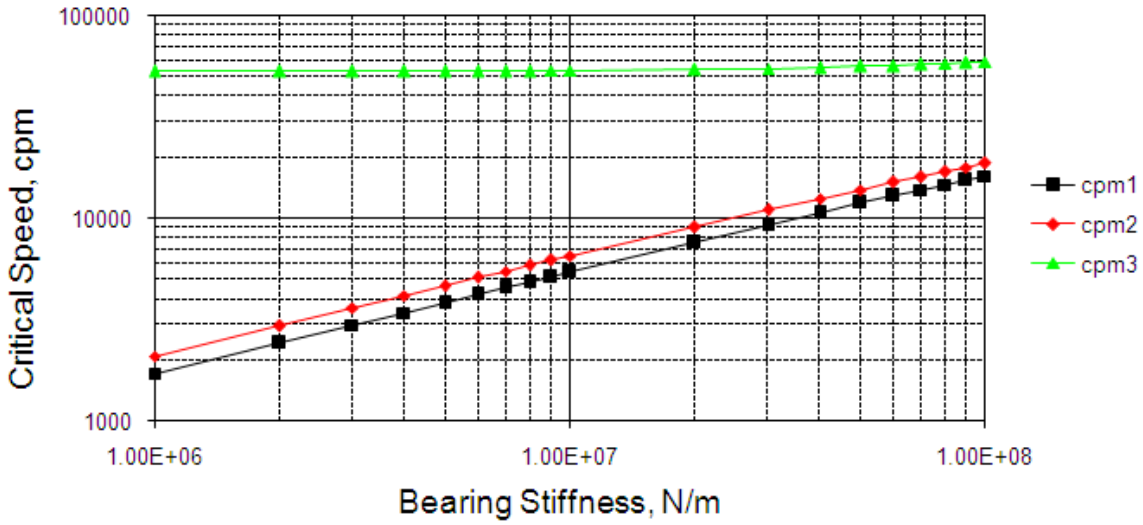

Figure 3.6 Undamped critical speed map for the stiffened rotor configuration.

The undamped critical speed map for the stiffer configuration is shown in Figure 3.6. The bearing stiffness of the front bearing is 42.6% of that of the rear bearings from the size ratio of the foil bearings to be used. The bearing stiffness of $10e^7$ N/m (rear foil bearing) yields the first 2 critical speeds about 5,400 and 6,500 rpm. The third critical speed (bending critical speed) of the stiffened engine is at 53,200 RPM giving a 20% margin above the maximum operating speed (44,700 RPM).

Figure 3.7 shows mode shapes of the first two critical speeds. Conical mode is excited about 5,400 rpm followed by a cylindrical mode about 6,500 rpm. A close resemblance to the critical speed and the mode of vibration is observed in the transient simulation as will be discussed in chapter 5.

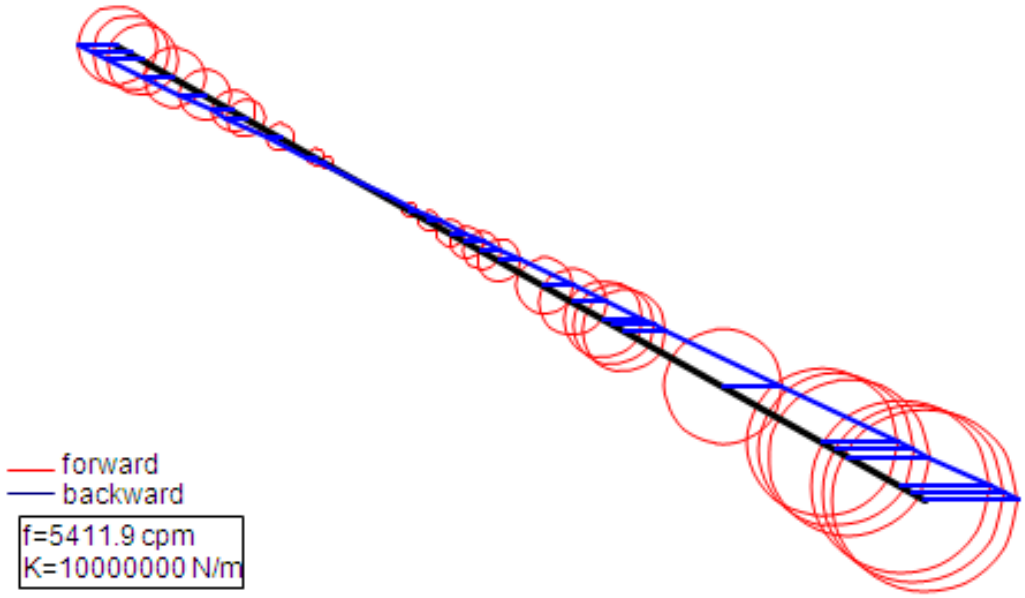

(a)

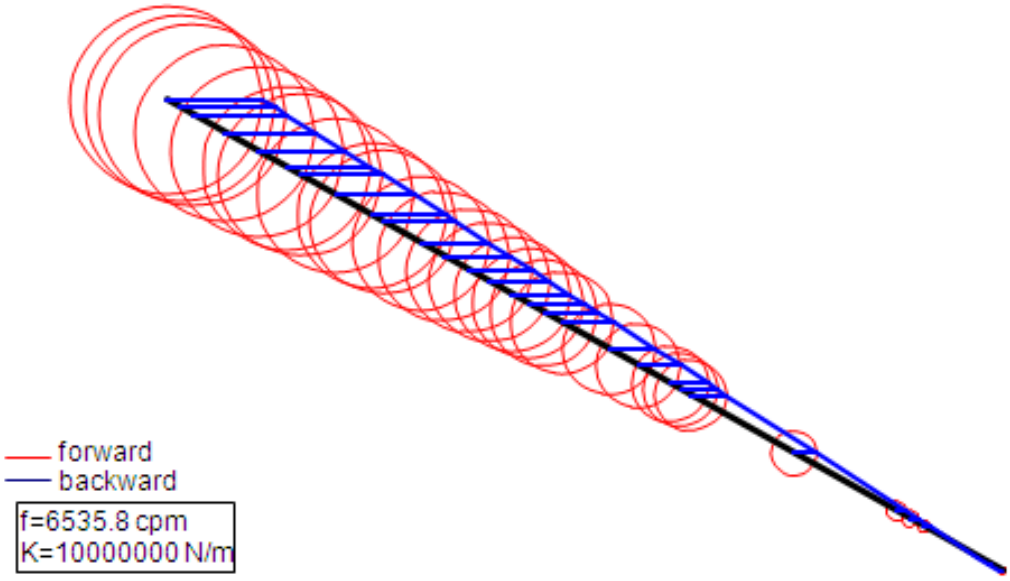

(b)

Figure 3.7 Mode shapes of the first two critical speeds (a) conical mode (b) cylindrical mode.

The new stiffened design shown in Figure 3.8 is installed with a thrust bearing next to the radial compressor impeller to accommodate the thrust loads. The thrust runner is modeled as added mass, and it does not contribute to the stiffness of the rotor. The modeled thrust runner weighs 4.91 Kg and 15mm wide.

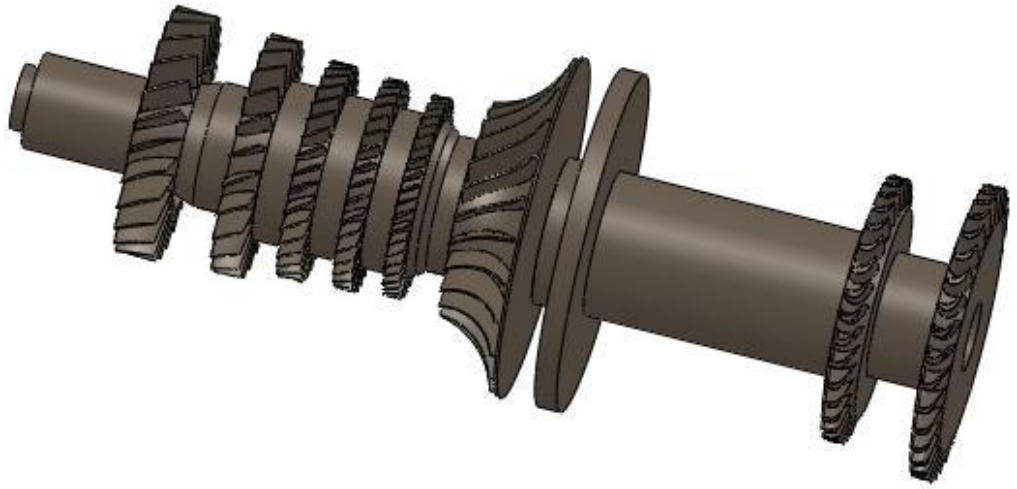

(a)

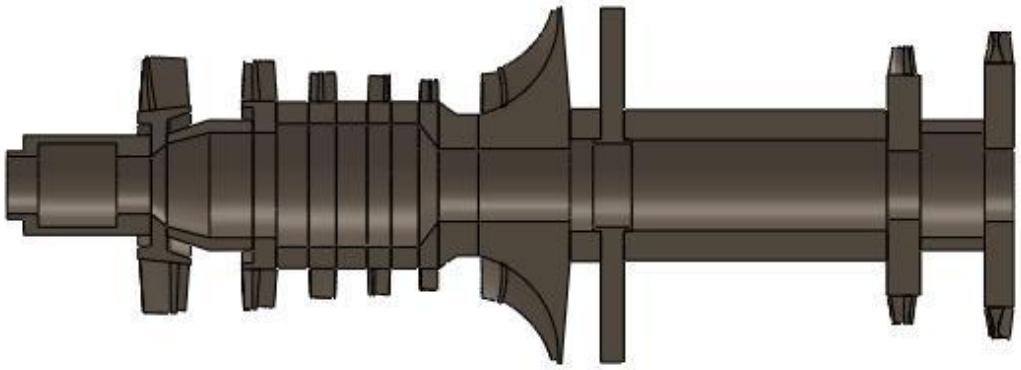

(b)

Figure 3.8 Stiffened solid model of T700 engine (a) Diametric view (b) Front section view

CHAPTER 4

MODELLING APPROACH FOR TRANSIENT SIMULATION

NASA's rotordynamic analysis was based upon linearized foil bearing dynamic force coefficients. The compliant structure (bump foil and the top foil) has been modeled as a single elastic foundation whose stiffness is assumed to be linear and constant everywhere. The stiffness and damping terms are calculated as the partial differential terms of the gas film forces acting on the journal. This method fails whenever there is a large displacement in the rotor orbit; the steady state is altered by highly nonlinear functions. In addition this method does not calculate the minimum film thickness.

This chapter explains the methodology adopted to obtain the imbalance response of the newly-designed T700 engine rotor, modeled as a rigid rotor with four DOF supported by two hybrid air foil bearings.

A numerical model has been developed to solve for the translational and angular gyroscopic motions of the rotor from the nonlinear equations of rotor motion and dynamic bearing reaction forces and moments from time dependent Reynolds equation. Using this developed numerical model, imbalance response of the system supported by different design parameters has been obtained. In addition minimum film thicknesses of the bearings in both conical and cylindrical mode were analyzed.

4.1. Transient Analysis

The stiffened T700 rotor is supported by 2 HAFBs, one in the cold section before the 5 stage axial compressor and the other in the hot-section right after the thrust runner. The co-ordinate system of the rotor bearing system of interest along with different variables denoting rotor motion is as shown in Figure 4.1

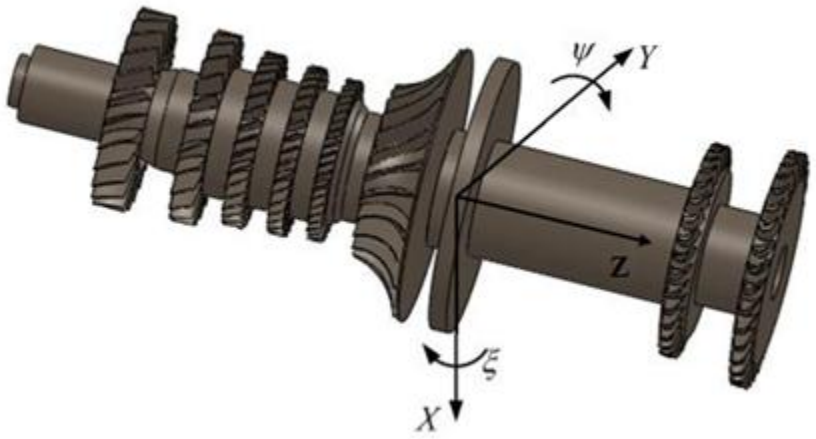

Figure 4.1 Coordinate system and variables for the simulation of the rotor motions

A four DOF rotor motions have been used to effectively evaluate the imbalance response for the conical mode. The system has two translational motions e_x and e_y, along X and Y direction respectively, two rotational motions ξ and ψ along X and Y direction respectively. These motions are derived by solving following governing equations.

EOM for radial motions,

$$\begin{aligned} m_r \ddot{e}_X &= m_r g + F_{X\_B} + F_{X\_U} \\ m_r \ddot{e}_Y &= F_{Y\_B} + F_{Y\_U} \end{aligned} \tag{1}$$

EOM for conical motions,

$$\begin{aligned} I_T \ddot{\xi} + I_P \omega \dot{\psi} &= M_{\xi\_B} + M_{\xi\_U} \\ I_T \ddot{\psi} - I_P \omega \dot{\xi} &= M_{\psi\_B} + M_{\psi\_U} \end{aligned} \tag{2}$$

In the equations (1) and (2), I_T and I_P are the translational and polar moment of inertia of the rotor respectively. F_{X_U}, F_{Y_U}, $M_{\square\_U}$ and $M_{\square\_U}$, represent the forces and moments induced by

imbalance mass of the rotor. F_{X_B}, F_{Y_B}, $M_{\square\_B}$ and $M_{\square\_B}$, represent the dynamic forces and moments induced by two hybrid foil bearings.

The forces and moments due to imbalance mass are given by equation (3) and equation (4);

$$\begin{Bmatrix} F_{X\_U} \\ F_{Y\_U} \end{Bmatrix} = \begin{Bmatrix} (mu)_1 \cos\omega t + (mu)_2 \cos(\omega t + \phi_p) \\ (mu)_1 \sin\omega t + (mu)_2 \sin(\omega t + \phi_p) \end{Bmatrix} \tag{3}$$

where $(mu)_1$ *and* $(mu)_2$ are the imbalances (with unit of mg-mm) located on the rotor, and Φ_p is the phase angle between the imbalances .

$$\begin{Bmatrix} M_{\xi\_U} \\ M_{\psi\_U} \end{Bmatrix} = \begin{Bmatrix} (mu)_1 \sin\omega t \cdot l_1 - (mu)_2 \sin(\omega t + \phi_p) \cdot l_2 \\ -(mu)_1 \cos\omega t \cdot l_1 + (mu)_2 \cos(\omega t + \phi_p) \cdot l_2 \end{Bmatrix} \tag{4}$$

where l_1 and l_2 are the axial distances between the center of mass of the rotor and imbalance locations.

The dynamic bearing reaction forces and moments are given by the following equations (5) and (6)

$$\begin{Bmatrix} F_{X\_B} \\ F_{Y\_B} \end{Bmatrix} = \begin{Bmatrix} \iint p_{j\_left} \cos\theta r d\theta dz + \iint p_{j\_right} \cos\theta r d\theta dz \\ \iint p_{j\_left} \sin\theta r d\theta dz + \iint p_{j\_right} \sin\theta r d\theta dz \end{Bmatrix} \tag{5}$$

$$\begin{Bmatrix} M_{\xi\_B} \\ M_{\psi\_B} \end{Bmatrix} = \begin{Bmatrix} -\iint z p_{j\_left} \cos\theta r d\theta dz - \iint z p_{j\_right} \cos\theta r d\theta dz \\ \iint z p_{j\_left} \sin\theta r z d\theta dz + \iint z p_{j\_right} \sin\theta r d\theta dz \end{Bmatrix} \tag{6}$$

Where p_{j_left} and p_{j_right} are the pressures developed in the fore bearing (at cold-section) and aft bearing (at hot-section) respectively.

These bearing reaction forces are calculated by solving transient-Reynolds equation, which is shown in equation (7).

$$\frac{\partial}{\partial x}\left(-\frac{1}{12\mu}\frac{p_j}{R_g T}h^3{}_j\frac{\partial p_j}{\partial x}+\frac{R\omega}{2}p_j h_j\right)+\frac{\partial}{\partial z}\left(-\frac{1}{12\mu}p_j h^3{}_j\frac{\partial p_j}{\partial z}\right)+\frac{\partial(p_j h_j)}{\partial t}=\frac{R_g T\dot{m}_s}{\Delta x\Delta z}$$

(7)

In the above equations, x is a local coordinate on the bearing surface representing the circumferential direction, z is the axial direction along the bearing from one edge to another, h_j is a film thickness, p_j is pressure, μ is viscosity of air, R_g is the gas constant of air and T is the temperature of the hydrostatic air and $\dot{m}_S$ is the mass flow rate through the orifice. $\dot{m}_S$ is modeled through isentropic nozzle as presented in[15]. The grid scheme for the control volume is shown in Figure 4.2

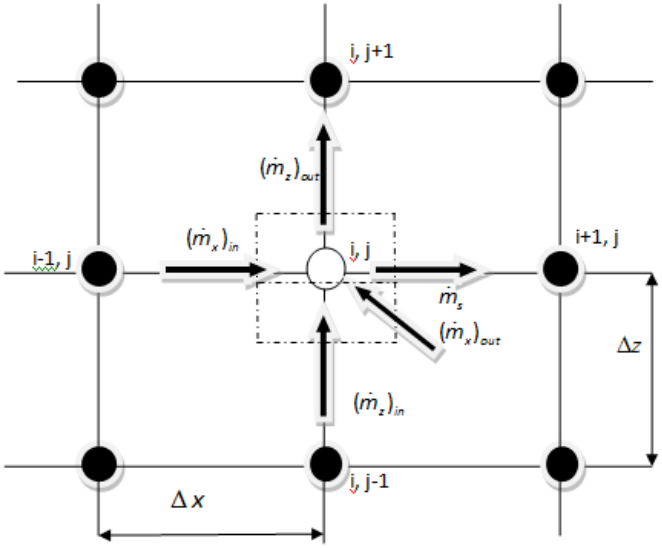

Figure 4.2 Finite volume mesh used for analysis

The classical formulation of Couette-Poiseuille flows, $\dot{m}_x$ and $\dot{m}_z$ are given as

$$\dot{m}_x = \left(-\frac{1}{12\mu} \frac{p_j}{R_g T} h^3{}_j \frac{\partial p_j}{\partial x} + \frac{p_j}{R_g T} \frac{h_j R\omega}{2} \right) \Delta z \tag{8}$$

$$\dot{m}_z = \left(-\frac{1}{12\mu} \frac{p_j}{R_g T} h^3{}_j \frac{\partial p_j}{\partial z} \right) \Delta x \tag{9}$$

Dynamic mass balance of the control volume under transient condition is given by

$$(\dot{m}_x + \dot{m}_z)_{in} + \dot{m}_s - (\dot{m}_x + \dot{m}_z)_{out} = \frac{d(\rho V)}{dx} = \frac{\Delta x \Delta z}{R_g T} \frac{d(p_j h_j)}{dt} \tag{10}$$

To enable the ease of computation equation (7) is non-dimentionalized as shown in equation (11). The variables used for non dimensionalization are as follows:

$$P_j = \frac{p_j}{P_a}, Z = \frac{z}{r_j}, \nu = \frac{\omega_s}{\omega}, \tau = \omega_S t, H_j = \frac{h_j}{C_j}, \Lambda_j = \frac{6\mu\omega}{p_a}\left(\frac{r_j}{C_j}\right)^2 \text{ and } \dot{M}_S = \frac{12\mu R_g T \dot{m}_s}{p_a{}^2 C_j{}^3}$$

$$\frac{\dot{M}_S}{\Delta\theta\Delta Z} + \frac{\partial}{\partial\theta}\left(P_j H_j{}^3 \frac{\partial P}{\partial\theta}\right) + \frac{\partial}{\partial Z}\left(P_j H_j{}^3 \frac{\partial P}{\partial\theta}\right) = \frac{\partial}{\partial\theta}\left(\Lambda_j P_j H_j\right) + 2\Lambda_j \nu \frac{\partial}{\partial\tau}\left(P_j H_j\right) \tag{11}$$

The film thickness of the journal bearing is given by (12)

$$h_j = C_j - r_{gc} + (e_X + \psi \cdot z)\cos\theta + (e_Y - \xi \cdot z)\sin\theta - r_p \cos\left(\theta - \theta_p\right) + \delta_j \tag{12}$$

where C_j is a nominal clearance of the journal bearing, r_{gc} is a centrifugal growth of rotor, r_p is a preload distance of each top foil pad (described in **Error! Reference source not found.**), and δ_j is a top foil deflection of journal bearing.

The rotor centrifugal growth is given by following equation.

$$r_{gc} = \frac{\rho_r r_j \omega^2}{4E}\left[r_j{}^2 (1-\nu)\right]$$

As seen in equation (12) the film thickness of the bearing is a function of the eccentricities (e_X,e_Y) of the rotor. Integrating the film pressure, the bearing reaction forces and moments (equations (5) and (6)) are obtained.

The Reynolds equation was solved by using the finite volume method. The grid size used for control volume was 44 and 14 in circumferential and axial direction per one top foil pad of the Two-pad journal bearing, and 30 in circumferential direction and 14 in axial direction per one top foil pad of Three-pad bearing. The rotor and bearing data considered for simulation is given in Table 4.1.

Table 4.1 Rotor and bearing data

Rotor	Length (l_r)	65 cm
	Mass (m_r)	35.6 kg
	Translational moment of inertia (I_T)	6.23 kgm^2
	Polar moment of inertia (I_p)	0.11 kgm^2
Front Journal bearing (2 pad)	Design type 1	
	Length (L_b)	50 mm
	Clearance (C_j)	250 µm
	Preload (r_p)	160 µm
	Bump stiffness	3.25 GN/m^3
Rear Journal bearing (2 pad)	Length (L_b)	75 mm
	Clearance (C_j)	350 µm
	Preload (r_p)	260 µm
	Bump stiffness	4 GN/m^3
Front Journal bearing (3 pad)	Design type 2	
	Length (L_b)	50 mm
	Clearance (C_j)	200 µm
	Preload (r_p)	30 µm
	Bump stiffness	3.25 GN/m^3
Rear Journal bearing (3 pad)	Length (L_b)	75 mm
	Clearance (C_j)	250 µm
	Preload (r_p)	80 µm
	Bump stiffness	4 GN/m^3

CHAPTER 5

RESULTS AND DISCUSSIONS

The imbalance response of 2 types of rotor bearing system designs have been simulated for a speed range of 4 to 50 krpm. In the first design uses two 2 pad bearings and the second design uses two 3 pad bearings. These tests were simulated in hydrostatic mode. Cylindrical and conical modes of vibrations were excited by applying imbalance mass at phase angles of 0° and 180°. The following Table 5.1 shows the details of imbalance mass and its modes of vibration. The selected imbalance mass 30,000 mg-mm falls under balance quality grade G2.5 according to the industrial standards (From ISO 1940/1), “Balance Quality Requirements of Rigid Rotors”.

Table 5.1 Imbalance mass location and modes of vibration being excited

Imbalance mass per bearing (mg-mm)	Location of imbalance mass from mass center of rotor (m)	Angular offset of imbalance mass	Mode of Vibration
30,000	-0.31	0°	Cylindrical
30,000	0.26	180°	Conical

The positive or negative sign given to the distance of imbalance mass indicates its location on the positive or negative Z axis (axial direction) considering the center of mass as origin.

5.1. Imbalance response in Hydrostatic mode for 2 pad bearing supports.

5.1.1. Conical mode

In general the conical mode instability is observed before cylindrical mode instability when the rotor has large I_T or when the distance between the bearings is small compared to the rotor length. The conical mode is excited by applying imbalances mass at two locations at an angular phase of 180°. The journal bearings are located at a distance of 53 cm. The vibration sensors are located at 37cm and 27cm on either sides of the center of mass of the rotor. The X direction (gravitational direction) and Y direction plots for the small bearing (bearing in cold-section) and big bearing (bearing in hot-section) are presented for 2 pad bearing design in this section.

Figure 5.1 shows the response at sensor 1. Bound sub-synchronous vibrations of frequency about 2,500 rpm and amplitude 1.6 µm starting at 35,000 rpm are observed, however these sub-synchronous vibrations steeply increase and loose bounds at 48,000 rpm.

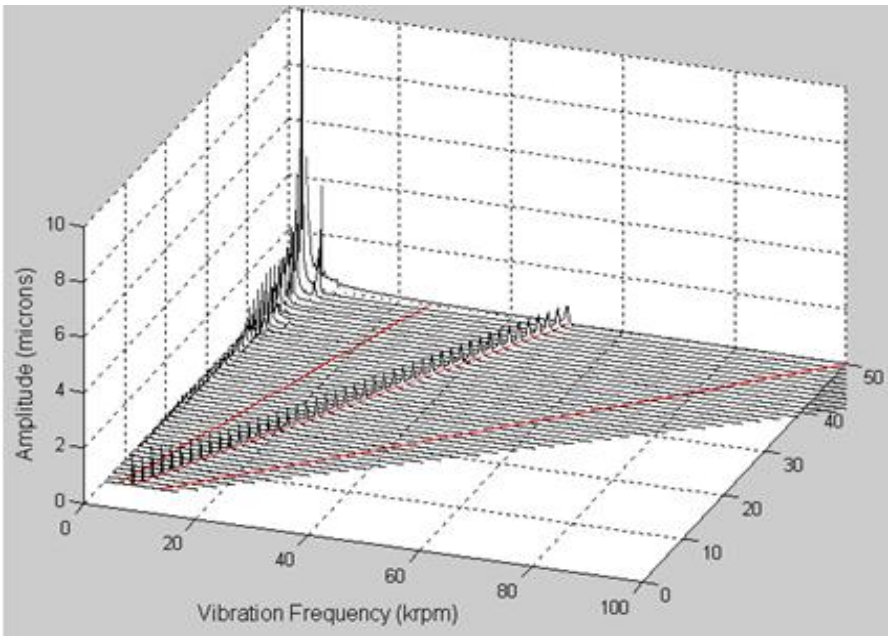

(a)

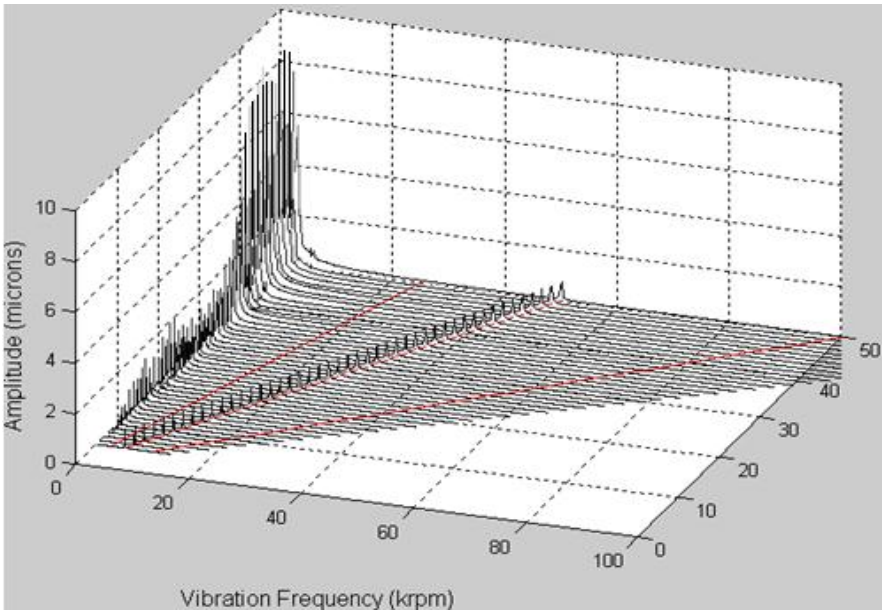

(b)

Figure 5.1 Out of phase imbalance response plot for design 1 at sensor 1(a) Vertical direction waterfall plot (b) Horizontal direction waterfall plot

The sub-synchronous vibrations in the Y direction start at 15,000 rpm, having amplitude about 1.6 µm. A rapid increase in the amplitude of sub-synchronous vibration from speeds over 40,000 is observed.

Figure 5.2 shows the response at sensor 3. The first noticeable sub-synchronous vibration appears at 36,000 rpm but with smaller amplitude of 0.7 µm compared to the vibration at sensor 1, yet similar pattern of sharp increase of the sub-synchronous vibration is observed for the later speeds.

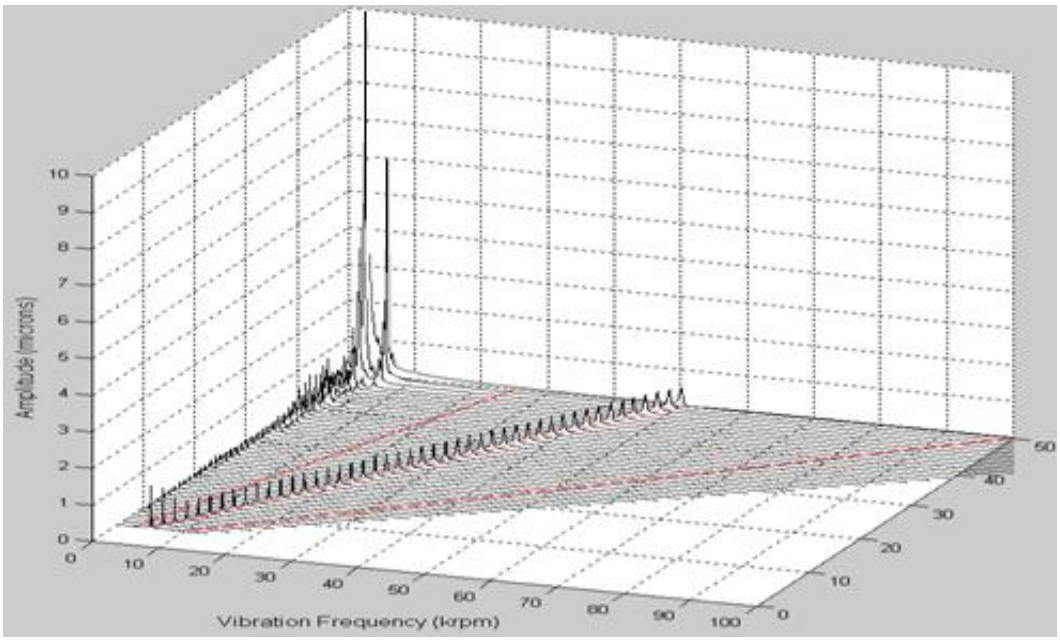

(a)

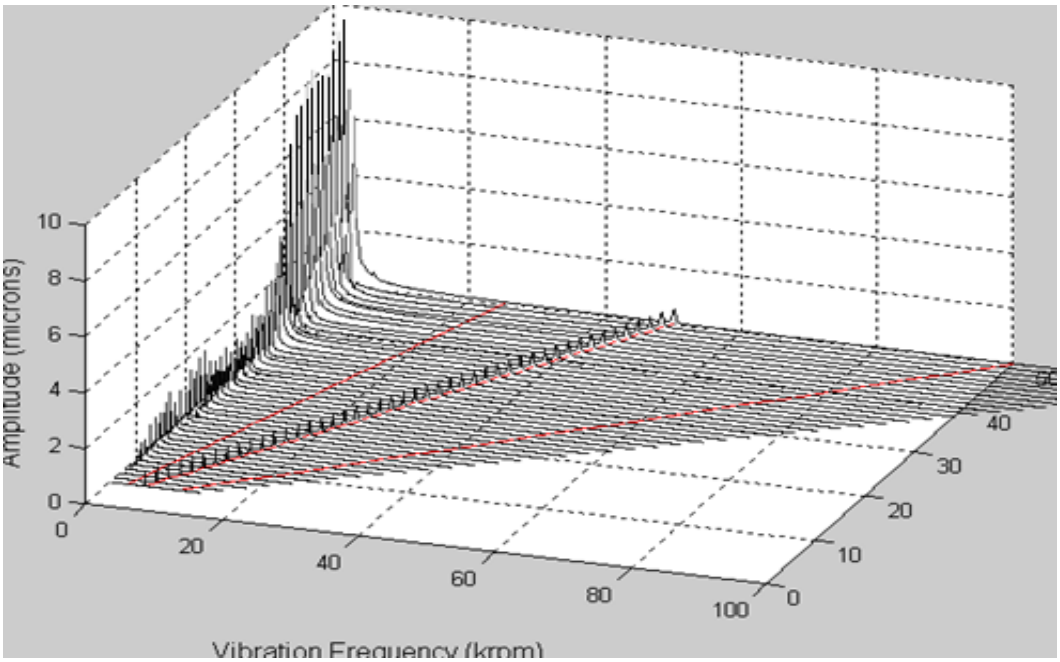

(b)

Figure 5.2 Out of phase imbalance response plot for design 1 at sensor 3(a) Vertical direction waterfall plot (b) Horizontal direction waterfall plot

The critical speeds for the small bearing and the big bearing shown in Figure 5.3 are noticed about speeds of 4,500 rpm, with a steady synchronous vibration starting from 25,000 rpm. The amplitudes of synchronous vibration at sensor 3 are greater compared to synchronous vibration at sensor 1.

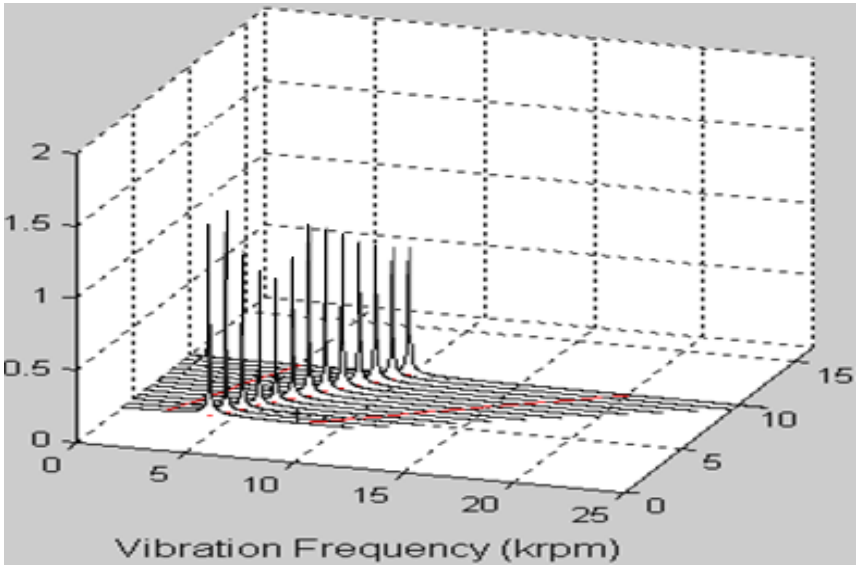

(a)

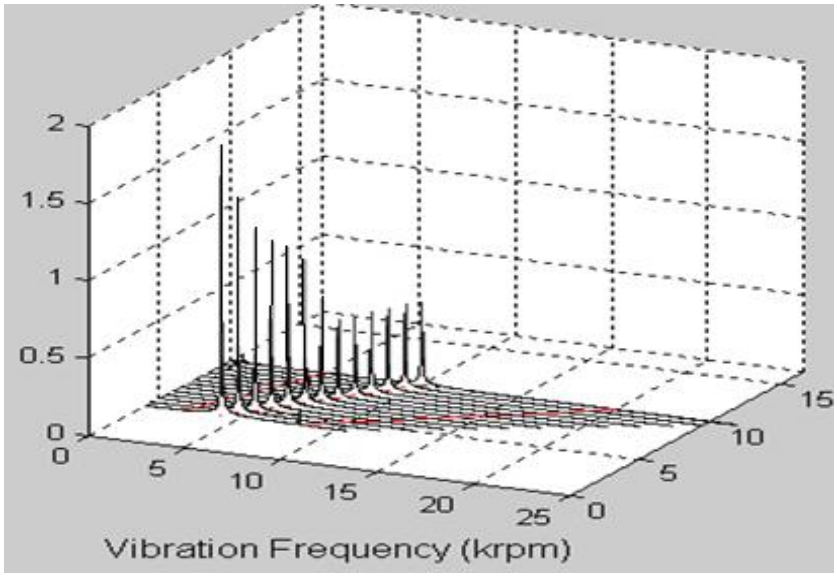

(b)

Figure 5.3 Out of phase imbalance response plots for speed range of 4 krpm to 10krpm (a) At Sensor 1 (b) At Sensor 3

5.1.2. Cylindrical mode

The sub-synchronous vibration at sensor 1 and sensor 3 follows a similar trend compared to sub-synchronous vibration in conical mode. It is observed from Figure 5.4 that critical speed appears about 7,000 rpm at a frequency of 7,000 rpm. Additionally it is noticed that the amplitude of the critical speed vibration at sensor 1 is slightly greater than vibration at sensor 3. A steady synchronous vibration is observed starting from 18,000 rpm at a magnitude of 1.3 µm.

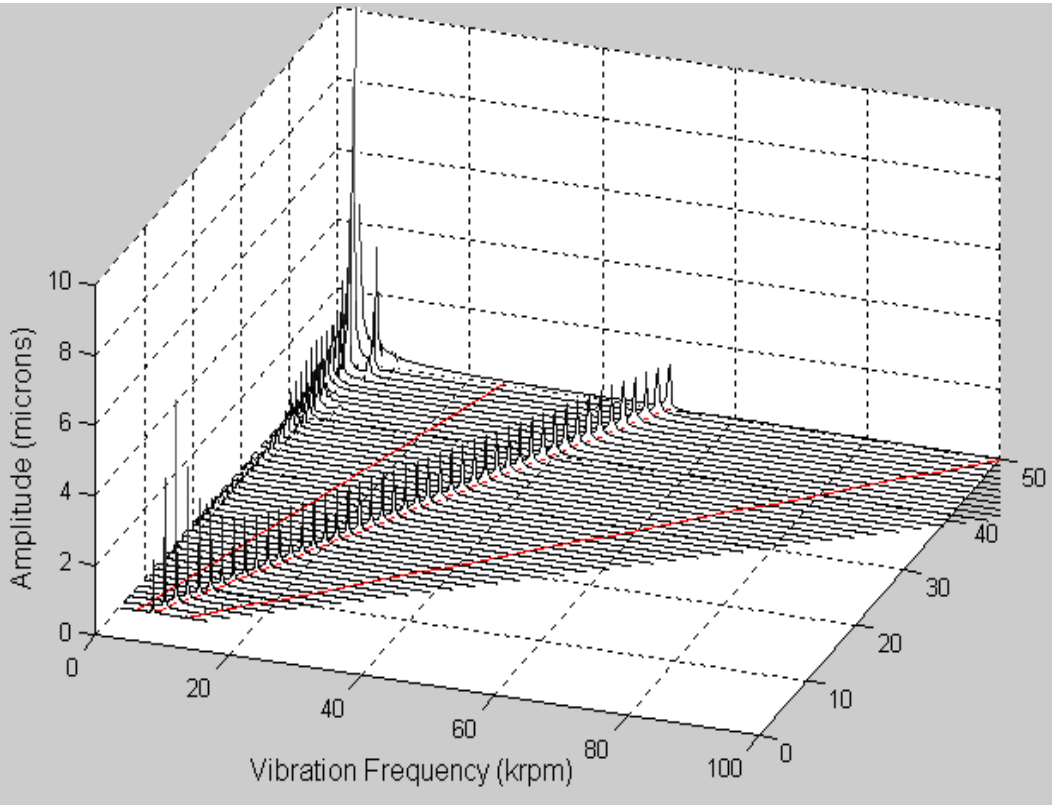

Figure 5.4 Waterfall plot for imbalance response in Cylindrical mode.

5.2. Imbalance response in Hydrostatic mode for 3 pad bearing supports.

5.2.1. Conical mode

The conical mode imbalance response plots for the big bearing in X and Y direction have been discussed in this section. The sub-synchronous vibration starts about 40,000 rpm. Though sub-synchronous vibrations are bound, they are considerably large compare to the 2 pad bearing in the X direction but are relatively small in the Y direction. Figure 5.5 shows the waterfall plots for vibrations picked up by sensor 3.

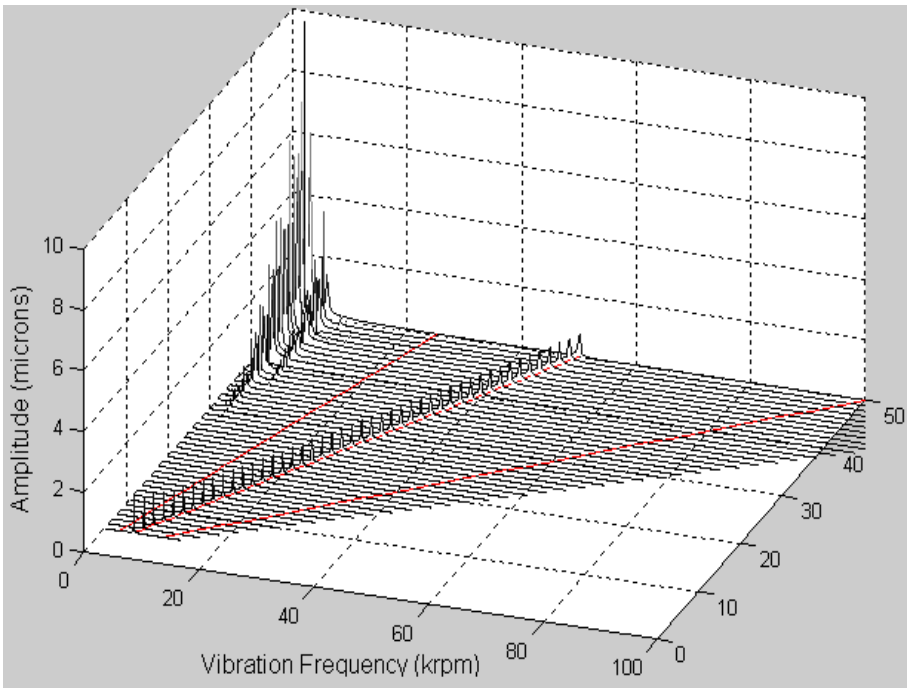

(a)

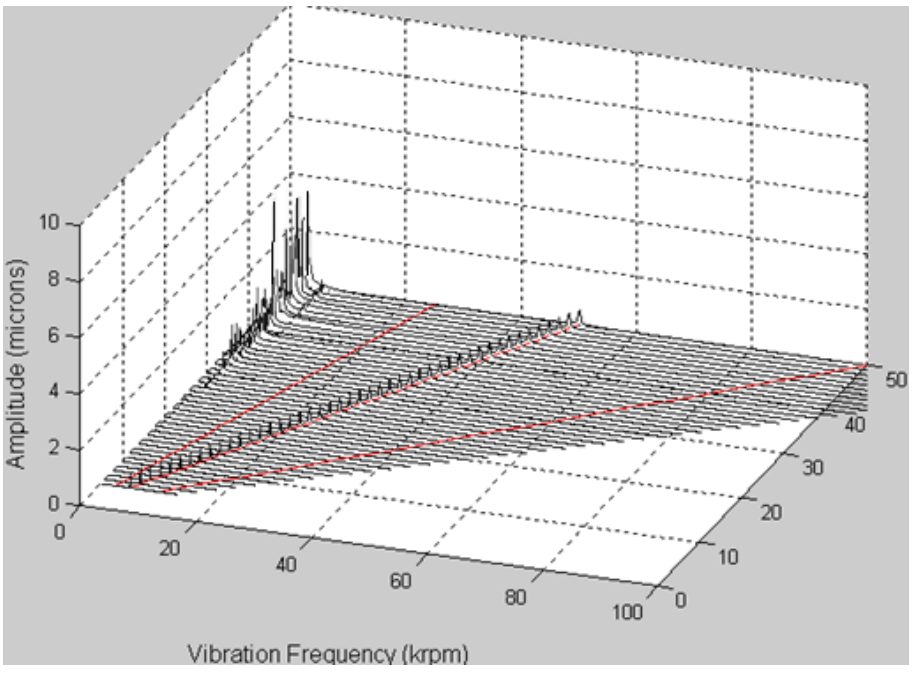

(b)

Figure 5.5 Out of phase imbalance response plot for design 2 at sensor 3(a) Vertical direction waterfall plot (b) Horizontal direction waterfall plot

5.2.2. Cylindrical mode

From the Figure 5.6 it can be noted that the sub-synchronous vibrations at sensor 3 are lesser in the horizontal direction than the vertical direction. This can be due to the stiffness variation due to gravitational loading in vertical direction.

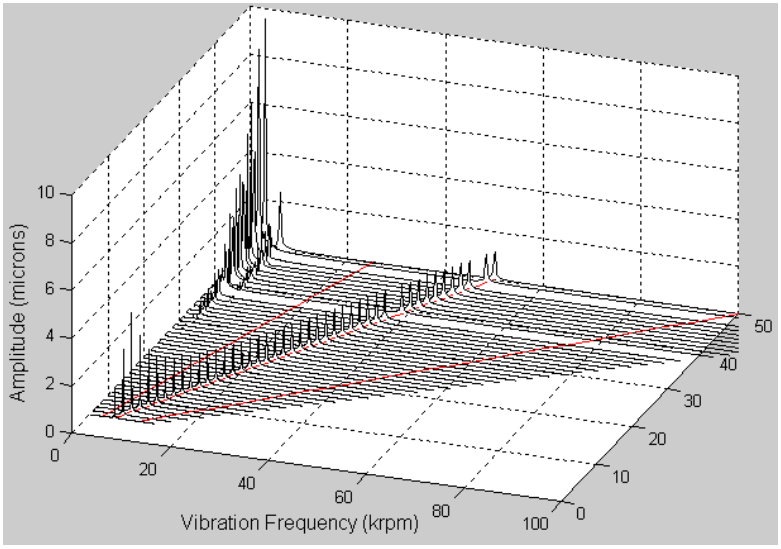

(a)

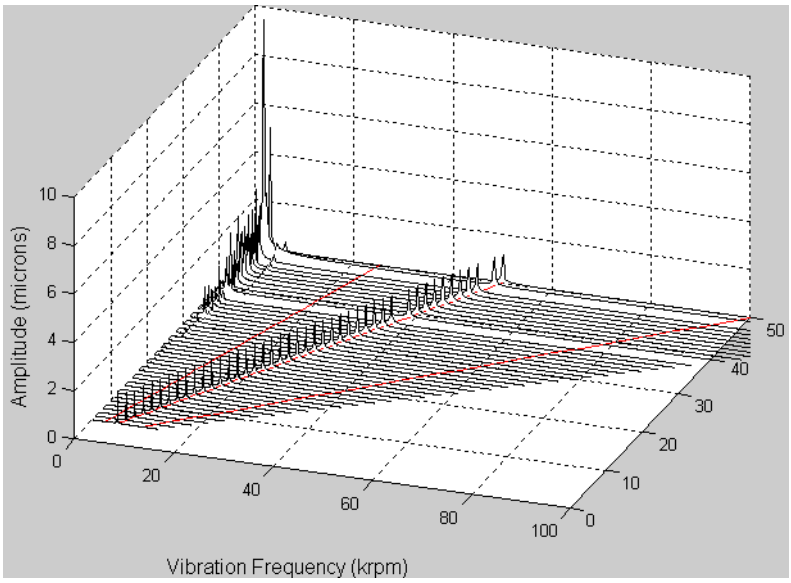

(b)

Figure 5.6 In phase imbalance response plot for design 2 at sensor 3(a) Vertical direction waterfall plot (b) Horizontal direction waterfall plot.

5.3. Effect of conical and cylindrical modes of vibration on film thickness

5.3.1. 2-pad bearing design

Figure 5.7 shows the minimum film thickness plots for 2 pad bearing design, throughout the speed range from 5krpm to 50krpm. It is observed that film thickness at both bearings in cylindrical mode drops about 7,000 rpm indicating the critical speed for this mode.

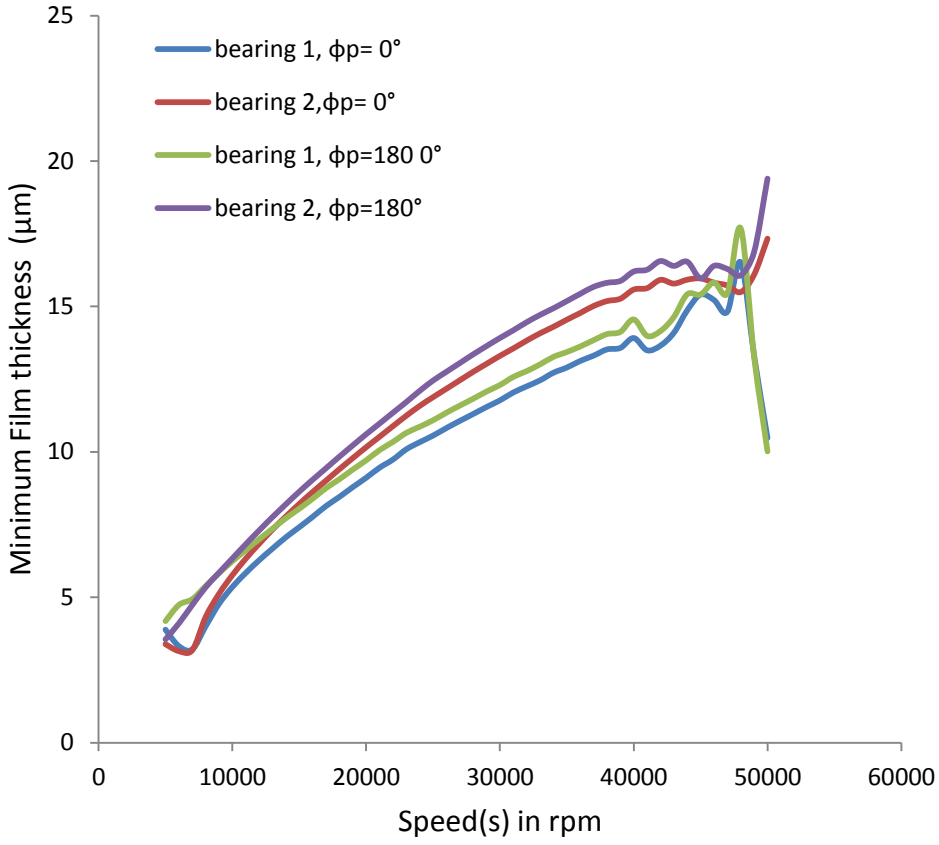

Figure 5.7 Minimum film thickness of the 2pad bearing at various $\Phi_{p.}$

5.3.2. 3-pad bearing design

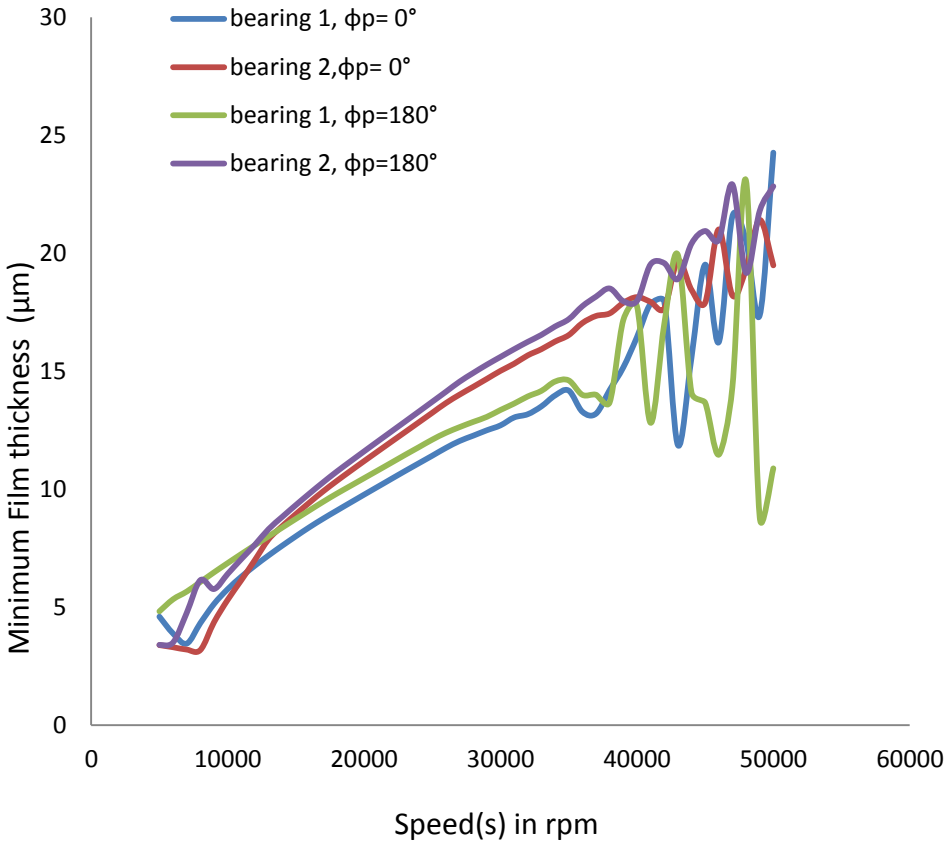

Figure 5.8 Minimum film thickness of 3 pad bearings at various $\Phi_{p.}$

The film thickness curve shown in Figure 5.8 increases as the speed increases, but starts fluctuating from speeds over 40 krpm due to increase in sub-synchronous vibrations in X Direction.

CHAPTER 6

CONCLUSION AND RECOMMENDATIONS

6.1. Conclusion

A new design of the GE T700 rotor supported by two different types of hybrid foil bearings has been investigated. Imbalance responses for a speed range of 5 krpm to 50 krpm under both conical and cylindrical modes have been simulated. Dynamic equations of rotor and transient Reynolds equations have been solved simultaneously to obtain the rotor motions.

The Critical speeds along the vertical direction (in both 3 pad and 2 pad designs) are observed to be greater than the horizontal direction, due to the gravitational loading. From the simulations it can be noted that the critical speeds for conical mode appears at about 4,000 rpm, and critical speeds for cylindrical mode appear at 7,000 rpm. The results agree well with the values obtained from the rotordynamic analysis software XL-Rotor®.

Though the amplitude of sub-synchronous vibrations for 3 pad bearing in X direction is slightly larger than 2 pad, it is relatively very less compared to the sub-synchronous vibrations in the Y direction. The Minimum film thickness plots for the bearing in the hot-section comparing both 2 pad and 3 pad designs shows that the film thickness in 3 pad bearing is larger than the 2 pad bearing. Thus between the two bearing designs, the 3 pad bearing is more acceptable. The capability to predict the film thickness is one significant advantage of the transient 4 DOF non-linear rotordynamic analysis.

6.2. Recommendations for future work

Considering a Flexible rotor model:

The rotor model in this article is considered to be rigid, and better analysis can be performed using the multi-degree of freedom (DOF) nonlinear analysis of a flexible rotor model. The entire

rotor can be modeled to a multiple station masses and mass-less stiffness elements connecting the station masses.

Consideration of thrust bearing forces and moments:

The axial thrust and loading factors can be considered, to obtain more refined imbalance response of the rotor bearing system.

Effects of start motor loading on the bearings:

Due to lack of data on the rated power of the start motor of the T700 engine, the radial loads to the shaft couldn't be calculated. If the radial load is known, more accurate transient behavior could be predicted.

BIBLIOGRAPHY

[1] Heshmat, H., 1993, "Role of Compliant Foil Bearings with in Advancement and Development of High-Speed Turbomachinery," 2nd ASME Pumping Machinery Symposium, Fluid Engineering Conference, June 20-24, 1993.

[2] Agrawal, G. L., 1997, "Foil Air/Gas Bearing Technology -- an Overview," International Gas Turbine & Aeroengine Congress & Exhibition, Orlando, FL, ASME Paper No. 97-GT-347.

[3] Swanson, E. E., Heshmat, H., and Walton, J., 2002, "Performance of a Foil-Magnetic Hybrid Bearing," Journal of Engineering for Gas Turbine and Power**, 124**(2), pp. 375-381.

[4] Anonymous *Chapter 10. General electric T700-GE-700*, US Army Aviation Logistics School, Fort Eustis, Virginia, pp. 256-262.

[5] Valco, M. J., and DellaCorte, C., "Emerging Oil-Free Turbomachinery for Military Propulsion and Power Applications," The Army Sciences Conference, Ft. Lauderdale, 2003.

[6] Howard, S. A., Bruckner, R. J., DellaCorte, C., and Radil, K. C., 2008, "Preliminary Analysis for an Optimized Oil-Free Rotorcraft Engine Concept," NASA Technical Report, NASA/TM—2008-215064.

[7] DellaCorte, C., and Valco, M. J., 2000, "Load Capacity Estimation of Foil Air Journal Bearings for Oil-Free Turbo-Machinery Applications," STLE Tribology Transaction**, 43**(4), pp. 795-801.

[8] Radil, K. C., and DellaCorte, C., 2009, "Foil Bearing Starting Considerations and Requirements for Rotorcraft Engine Applications," Army Research Laboratory Technical Report, ARL-TR-4873.

[9] DellaCorte, C., Lukaszewicz, V., Valco, M. J., Radil, K. C., and Heshmat, H., 2000, "Performance and Durability of High Temperature Foil Air Bearings for Oil-Free Turbomachinery," NASA Technical Report, TM-2000-209187/ARL-TR-2202.

[10] Howard, S. A., Bruckner, R. J., and Radil, K. C., 2010, "Advancements Toward Oil-Free Rotorcraft Propulsion," NASA Technical Report, NASA/TM—2010-216094.

[11] Radil, K., Howard, S., and Dykas, B., 2002, "The Role of Radial Clearance on the Performance of Foil Air Bearings," STLE Tribology Transaction**, 45**(4), pp. 485-490.

[12] Lee, D., and Kim, D., 2010, "Five Degrees of Freedom Nonlinear Rotor Dynamics Model of a Rigid Rotor Supported by Multiple Airfoil Bearings," Proceedings of the 8th IFToMM International Conference on Rotordynamics, Seoul, Korea, September 12-15, Paper No. WeD1-2.

[13] Kim, D., and Lee, D., 2010, "Design of Three-Pad Hybrid Air Foil Bearing and Experimental Investigation on Static Performance at Zero Running Speed," Journal of Engineering for Gas Turbine and Power**, 132**(12), pp. 122504-1~10 (10 pages), DOI:10.1115/1.4001066.

[14] Kumar, M., and Kim, D., 2010, "Static Performance of Hydrostatic Air Bump Foil Bearing," Elsevier Tribology International**, 43**(4), pp. 752-758, doi:10.1016/j.triboint.2009.10.015.

[15] Kumar, M., and Kim, D., 2008, "Parametric Studies on Dynamic Performance of Hybrid Air Foil Bearings," Journal of Engineering for Gas Turbines and Power**, 130**(6), pp. 062501-1-062501-7.

BIOGRAPHICAL INFORMATION

Mahesh Kumar Varrey was born in Secunderabad, India on October 18, 1987. He received his Bachelor degree from Anna University, Chennai, in Mechanical Engineering in 2005. He joined University of Texas at Arlington in 2009 to pursue a Master of Science in Mechanical Engineering. His interests include Rotordynamics, Finite element method and Computer Aided Design.